

Chapter 6

How Metamorphism Affects Iron Mineralogy and the Iron Speciation Redox Proxy: a Data-Driven Theoretical Study

Coauthors:

John M. Eiler and Woodward W. Fischer

6.1 Abstract

As the most abundant transition metal in the Earth's crust, iron controls the planetary redox budget. Observations of iron minerals in the sedimentary record have been used to understand surface atmospheric and aqueous redox environments over the evolution of our planet; today, the most popular method is iron speciation, a geochemical sequential extraction proxy calibrated to modern sediments. We tested the limits of this proxy to understand the mobility of iron in sediments post-deposition by utilizing data from two classic well-understood localities where Silurian-Devonian shales, sandstones, and carbonates deposited in oxic conditions have been regionally metamorphosed from lower-greenschist facies to granulite facies: Waits River and Gile Mountain Formations, Vermont and the Waterville and Sangerville-Vassalboro Formations, Maine. Plotting iron speciation ratios determined for samples from these localities revealed apparent paleoredox conditions of the depositional water column spanning the entire range from oxic to ferruginous (anoxic) to euxinic (anoxic and sulfidic.) The presence of diagenetic iron carbonates in the samples severely affected the proxy even at low grade, creating ferruginous conditions in all lithologies especially in carbonate rocks. Increasing metamorphic grades transformed iron in carbonates into iron in silicate minerals, which when combined with a slight increase in pyrrhotite, resulted in reconstructed conditions being driven more oxic and more euxinic. Metamorphic reactions involving iron were offset between carbonate and siliciclastics and could be abrupt between metamorphic facies or more gradual in nature. Comparison with previously published metamorphic transformations highlighted the many ways in which the iron speciation proxy can be affected with increasing grade; notably, our work highlights the importance of trace iron in phases which otherwise might not be included when studying the iron systematics of a region. Iron is incredibly mobile and reactive during diagenesis and metamorphism, and subsequent processes can easily overprint primary redox information. Detailed geologic field observations and petrographic

work to understand alteration and metamorphism are important tools needed for understanding paleoenvironmental conditions on Earth.

6.2 Introduction

Iron is by far the most abundant transition metal in the crusts of rocky planets, planetary bodies, and asteroids (Lodders and Fegley, 1997), and it buffers (bio)geochemical processes and redox state on a planetary scale. As a redox-sensitive element that cycles between +II and +III valence states, the abundance of different Fe phases within rocks can provide a window into the redox balance and oxygen levels/fugacity of the formation environment—whether it be deep in the mantle or on the surface within a sedimentary basin. Therefore, iron has played a central role in studies of Earth's development over the past 4.5 billion years into a life-sustaining, oxygen-rich planet.

Early observations of changing iron abundance and mineralogy in sedimentary rocks documented the rise of atmospheric oxygen based on the transition from ferrous to ferric iron-bearing detrital minerals and paleosols leached of soluble Fe^{+2} versus accumulation of insoluble Fe^{+3} (Cloud, 1968; Holland, 1984; Roscoe, 1969). Key evolutionary innovations have been linked to the rise of atmospheric oxygen (e.g. Johnson et al., 2013; Kopp et al., 2005; Williamson et al., 2011), and it is clear that this global environmental change dramatically altered evolutionary pathways for early life (Sleep and Bird, 2008). On the microscale, changes in redox state of the Earth's atmosphere and oceans changed the proportions of the metals used in enzymes for early life (Anbar, 2008; Williams and Frausto Da Silva, 2003; Zerkle et al., 2005). Therefore, the question of redox state of the atmospheres and oceans during the Precambrian has become a research priority in recent years in order to help understand the environmental controls on the pacing of evolution.

A variety of geochemical techniques have been applied to understand paleoredox based on diverse transition metal abundances and isotopologues; one of the most popular proxies is iron speciation. Iron speciation is a bulk sequential

chemical extraction technique to quantify the proportions of different iron phases, which are interpreted using empirical calibrations of modern sedimentary environments to determine paleoredox state of the depositional environment: oxic, anoxic/ferruginous (< 5 micromolar O_2), or euxinic (anoxic and sulfide bearing) (Poulton and Canfield, 2005; Raiswell and Canfield, 2012). Iron speciation data on a multitude of Precambrian successions suggest ferruginous, euxinic, and oxic waters varying between different basins, different water depths, and temporally with dominant ferruginous conditions (e.g. Poulton and Canfield, 2011; Sperling et al., 2015) distinctly different and far more complex than the canonical view (ferruginous before 2.3 Ga, then oxic surface waters with deep ocean euxinia) (Canfield, 1998; Cloud, 1968). Additionally, other paleoenvironmental proxies (such as Mo isotopes) have used the redox interpretations from iron speciation as a basic assumption to develop their methodology and build their interpretation models (e.g. Arnold et al., 2004; Kendall et al., 2009). However, since iron speciation is calibrated for sediment, it is poorly understood how metamorphism, metasomatism, and diagenesis could alter results and paleoenvironmental interpretations, an important caveat since all Precambrian rocks have undergone post-depositional alteration. Our approach analyzed case examples of sedimentary strata, which have undergone a range of well-understood metamorphic transformations, in “iron speciation space” to understand the effects of metamorphism on iron mineralogy and the iron speciation proxy.

6.3 Background

6.3.1 Development of the Iron Speciation Proxy

The iron speciation paleoredox proxy developed from work by Bob Berner and his students and colleagues at Yale to understand controls on the formation of pyrite in modern environments (Raiswell and Canfield, 2012). Iron is classified broadly into three hierarchical pools: pyrite iron (Fe_{py}), highly reactive (toward sulfide) iron (Fe_{HR}), and total iron (Fe_T). The ratio of Fe_{HR}/Fe_T is used to determine whether the depositional water column is oxic or anoxic, and then

within those that are anoxic, the ratio of Fe_{py}/Fe_{HR} is used to determine euxinic versus ferruginous water conditions (Fig. 6.1). As the proxy has evolved and been refined, different chemical extraction techniques have been used to resolve the various pools of iron (Table 6.1) adding a layer of complexity when applying or interpreting the proxy, which was originally operationally-defined based on the extraction steps.

The development of Fe_{py}/Fe_{HR} as an indicator for euxinic conditions is based on the Degree of Pyritization (DOP) ratio defined by Berner (1970). DOP and Fe_{py}/Fe_{HR} are both statistics measuring how much of the reactive iron in a sample has been transformed to pyrite iron. The distinction between these proxies is that DOP defines Fe_{HR} as pyrite iron plus iron extracted using boiling HCl while today, alternative extraction methods for Fe_{HR} have become widely utilized (e.g. Leventhal and Taylor, 1990; Poulton and Canfield, 2005; Raiswell et al., 1994). DOP was calibrated as euxinic if greater than 0.75 and oxic if less than 0.45 based on a survey of Cretaceous, Jurassic, and Devonian shales whose paleoenvironment was determined based on bioturbation and faunal assemblages (Raiswell et al., 1988). A later survey of modern siliciclastic sediments suggested that a $DOP < 0.4$ indicated oxic environments, but many euxinic environments had $DOP < 0.75$, interpreted as being due to additional transformation of iron oxides into pyrite during diagenesis in euxinic systems (Raiswell and Canfield, 1998). As studies moved toward using Fe_{HR} extractions when HR is extracted using dithionite instead of just boiling HCl, calculations were performed for Fe_{py}/Fe_{HR} to show that Fe_{py}/Fe_{HR} is on average 0.87 for euxinic deep Black Sea samples, 0.65 for Black Sea shelf sediments, and 0.61 for dysoxic marine samples (data from Anderson and Raiswell, 2004; Raiswell and Canfield, 1998). From this data, an upper limit of $Fe_{py}/Fe_{HR} = 0.8$ was chosen for ferruginous conditions (Poulton and Canfield, 2011; Raiswell and Canfield, 2012). No further calibrations on large surveys of sediment or rocks have been done with the standard detailed sequential extraction technique for Fe_{HR} (Poulton and Canfield, 2005). However, a study on Cretaceous marine shale from Ocean Anoxic Event 3

independently defined euxinia based on lack of bioturbation and presence of sulfurized organic matter and trace elements (Cd, V, Mo, Zn) as a test of the proxy; ratios of Fe_{py}/Fe_{HR} corroborated the upper limit of 0.8 and suggested a lower limit of euxinia at $Fe_{py}/Fe_{HR}=0.7$ (März et al., 2008). These limits have become the standard (Fig. 6.1), and have been widely applied to differentiate euxinic and ferruginous conditions of Precambrian-age rocks (Fig. 6.2) (Poulton and Canfield, 2011; Raiswell and Canfield, 2012).

Although the anoxia proxy was developed independently, today most studies pair the Fe_{HR}/Fe_T anoxia proxy with the Fe_{py}/Fe_{HR} euxinia proxy discussed above (first done by Shen et al., 2002). The primary focus of the Raiswell and Canfield (1998) modern siliciclastic sediment survey was to understand the abundances of highly-reactive iron (extracted using dithionite). They discovered a range of $0.06 < Fe_{HR}/Fe_T < 0.38$ bound oxic and dysoxic sediments. Samples from modern euxinic and anoxic basins contained Fe_{HR}/Fe_T ratios primarily above 0.38, but included values down to 0.18. Phanerozoic shales deposited in normal oxic marine conditions, based on faunal assemblages and DOP values, had a Fe_{HR}/Fe_T average of 0.14 significantly lower than the modern sediment average of 0.26 (Poulton and Raiswell, 2002). Additionally, a detailed test of Fe_{HR}/Fe_T on the Jurassic Kimmeridge Clay highlighted that Fe_{HR}/Fe_T ratios tracked well with oxygen limitation and anoxia as determined by faunal assemblages and bioturbation (Raiswell et al., 2001). Based on these compilations, the paleo-proxy was defined as having a lower Fe_{HR}/Fe_T limit of 0.22 chosen for anoxic sediments and an upper limit of oxic conditions at 0.38 (Fig. 6.1) (Poulton and Canfield, 2011). Notably, the Fe_{HR}/Fe_T limits have not been updated for the new sequential extraction techniques, although a test on modern carbonate samples from a range of oxic and anoxic environments using the new sequential extraction technique suggested that the Fe_{HR}/Fe_T limits were similar (Clarkson et al., 2014). Re-evaluation of the low Phanerozoic shale average compared to the modern sediment average raises the question as to whether samples are in an open system (previous assumption) or a closed system, where highly reactive iron was

transformed into iron minerals targeted in newer extraction methods or was moved into clays and the unreactive silicate pool (Raiswell and Canfield, 2012).

6.3.2 Sequential Extraction Pools

Bulk geochemical extraction techniques help provide quantitative results, and have allowed the development of this paleoredox proxy. However, questions always exist as to whether the targeted phases are being extracted or not; this is exemplified through the development of the highly reactive iron extraction techniques over the past 30 years within the iron speciation proxy. Today most studies follow the sequential extraction technique developed by Poulton and Canfield (2005) with slight modifications depending on the samples, mineralogy, and personal preference. This technique keeps Fe_{py} the same and divides the Fe_T and Fe_{HR} pools as such:

$$Fe_{HR} = Fe_{carb} + Fe_{ox1} + Fe_{ox2} + Fe_{mag} + Fe_{py}$$

$$Fe_T = Fe_U + Fe_{PRS} + Fe_{HR}$$

where Fe_{carb} is the iron carbonate pool, Fe_{ox1} and Fe_{ox2} combined are the ferric iron oxide pool, Fe_{mag} is the magnetite pool, Fe_U is the unreactive pool, and Fe_{PRS} is the poorly reactive sheet silicates (see Table 6.1 for additional details). The addition of these extra extraction steps was to target magnetite and iron-rich carbonates, which might precipitate in the water-column or in diagenesis from original reactive iron in Precambrian rocks and be of importance for paleoenvironmental interpretations (Poulton and Canfield, 2005; Raiswell and Canfield, 2012).

Even with these new targeted phases, there are still several iron-bearing (and sulfur-bearing) minerals present in ancient rocks that can be extracted during the iron speciation steps, but are not explicitly defined (e.g. Tables 6.1, 6.2). Notably, pyrrhotite is entirely or partially dissolved during the Fe_{carb} extraction (Poulton and Canfield, 2005; Reuschel et al., 2012), potentially with more extracted in the Fe_{mag} extraction (Burton et al., 2006), and can also be extracted in the Fe_{py} pool (Partin et al., 2015; Praharaj and Fortin, 2004; Schumann et al.,

2012); therefore additional extraction steps and calculations are often included when pyrrhotite is present. Pyrrhotite, if tested for separately, is usually grouped within the Fe_{py} pool in a new sulfurized iron pool (Fe_s) with the assumption that it formed from pyrite and/or represents original euxinic conditions on its own (e.g. Asael et al., 2013; März et al., 2008; Reuschel et al., 2012). An additional complexity with chemical extraction techniques is that some work has suggested the abundance of minerals or mixture of minerals within samples can affect extraction recovery (Hsieh et al., 2002; Praharaj and Fortin, 2004; Reuschel et al., 2012). Recent concern about the Poulton and Canfield (2005) method for iron speciation involves samples with high proportions of siderite and ankerite; in these samples, siderite is not fully extracted in the Fe_{carb} step and can continue to be extracted during the Fe_{mag} and Fe_{PRS} steps, which in the latter case will affect the iron speciation paleoredox proxy (Raiswell et al., 2011; Reinhard et al., 2009).

6.3.3 Previous Adjustments and Models for Metamorphism

As the iron speciation proxy has been developed, it has been applied to more diagenetically altered and metamorphosed samples, sometimes with detailed discussion, additional extractions, or petrography to understand how the iron moved during diagenesis/metamorphism and to attempt to recreate the original iron pools. Testing for pyrrhotite is one such adjustment, although calculation of “original” iron can be difficult since pyrrhotite has variable stoichiometry and in AVS and CRS extractions for sulfides, the sulfur is measured not the iron. Studies sometimes attempt to calculate pyrrhotite stoichiometrically (e.g. Asael et al., 2013; Cabral et al., 2013) while other times it is simply grouped with pyrite using stoichiometric equations that will under-estimate the amount of iron (e.g. Li et al., 2015; Partin et al., 2015). The question of authigenic syndepositional or diagenetic pore-water phases has begun to be addressed by Raiswell et al. (2011) who provided additional extraction tools with which to calculate poorly reactive silicates such as mica and chlorite and to more precisely measure iron carbonate phases. Although this method allows more precise determination of Fe_{carb} , iron

from the authigenic sheet silicate pool is interpreted using other geochemical proxies as simple delivery of hydrothermal Fe into an open system with no additional calculations or adjustments to Fe_{HR}/Fe_T . Studies on paired limestone and dolomite samples from early Triassic carbonates show an increase in Fe_{HR}/Fe_T ratios and Fe_{carb} in the dolomites due to deep burial dolomitization, and modern samples with low total iron (<0.5 wt%) also show enrichments in Fe_{HR}/Fe_T above the 0.38 oxic limit, interpreted to be from diagenetic dolomitization or pyrite formation (Clarkson et al., 2014).

The effect on iron speciation of iron movement between the silicate, highly reactive, and pyrite pools has been addressed through simple models. Transformation of carbonates and oxides to silicate phases will lower Fe_{HR}/Fe_T values and increase Fe_{py}/Fe_{HR} values as will the authigenic formation of iron silicates, making paleoredox appear more oxic and more euxinic (Reinhard et al., 2013). The formation of pyrrhotite from pyrite by loss of sulfur from the system without any iron transformations will lower Fe_{HR}/Fe_T and Fe_{py}/Fe_{HR} ratios in ferruginous systems making basins appear more ferruginous and/or more oxic; if iron sulfides are the main highly-reactive mineral, possible in some euxinic environments, less of a shift in Fe_{py}/Fe_{HR} toward ferruginous conditions would be seen (Reinhard et al., 2013). In this study, we expanded upon this previous work by considering additional iron reactions, using data from metamorphosed rocks as test-cases, and increasing the span of studied metamorphic conditions.

6.4 Approach

6.4.1 Locality Selection

We combed the literature for publications with detailed mineral assemblages of sedimentary rocks, preferably fine-grained siliciclastics, across a metamorphic gradient. Due to the low-abundance of iron in shales (<7 wt%, e.g. Li and Schoonmaker, 2003), accessory minerals needed to be carefully tabulated as well, excluding normative XRF analyses. Many iron-bearing carbonates and silicates such as chlorite and biotite have variable stoichiometries, and therefore,

mineral chemical composition also needed to be analyzed for each mineral in each rock sample. Several hundred metamorphic petrology papers were evaluated, but less than 30 publications fit the criteria established above. Two geologic locations stood out as particularly well-studied, the metamorphosed Silurian-Devonian sedimentary rocks of Vermont and Maine, so we focused on them. It is important to note that the sedimentary protoliths of these rocks were deposited as interbedded sandstones, shales, and carbonates in Paleozoic coastal marine settings; this type of setting is interpreted to be oxic even in benthic sediments based on other localities which contain abundant aerobic animal fossils (brachiopods, corals, echinoderms, etc.) (Watkins, 1996).

6.4.1.1 Waits River and Gile Mountain Formations, Vermont

The Waits River and Gile Mountain Formations of Vermont are a classic case of the Barrovian metamorphic series spanning from the chlorite to the kyanite zone. The Waits River Formation is composed predominately of tan siliceous limestone interbedded with calcareous black sulfidic shales, while the overlying Gile Mountain Formation contains grey sandstones and shales with some interbedded black shales and rare carbonate beds (Fisher and Karabinos, 1980; Hatch, 1988; Lyons, 1955; Woodland, 1977). The proportion of carbonate beds in the Waits River Formation increases to the east (Hatch, 1988). Layers in both formations are on the centimeter to decimeter scale (Fisher and Karabinos, 1980). The sequence is dated to Silurian and early Devonian based on Devonian plant fossils in the Gile Mountain Formation and a felsic dike through volcanics within the Waits River Formation having a zircon age of 423 ± 4 Ma (Hueber et al., 1990). Although fairly unfossiliferous, a poorly preserved echinoderm was found in the Waits River Formation (Hueber et al., 1990). The Waits River and Gile Mountain Formations were folded, intruded by granitic plutons, and then regionally metamorphosed during the Devonian Acadian orogeny (Osberg et al., 1989; Thompson and Norton, 1968; Thompson et al., 1968). Hornblendes dated using Ar-Ar in and near structural domes are between 350 and 397 Ma confirming

the age of this metamorphism (Spear and Harrison, 1989). Based on the minerals in the pelitic schists, preserved rocks were metamorphosed following the Barrovian series from the chlorite zone through the biotite, garnet, staurolite and kyanite zones (Doll et al., 1961; Ferry, 1994). Within the metamorphosed carbonate rocks of the Waits River Formation, isograds and zones were mapped based on the presence of ankerite, oligoclase, biotite, amphibole, and diopside (Ferry, 1992). Temperature conditions ranged from 400-450°C in the chlorite zone with similar temperatures for the ankerite-albite zone up to 525-575°C in the diopside and kyanite zones (Ferry, 1988b, 1992, 1994; Léger and Ferry, 1993). Pressure estimates vary from 3.5 to 7.8 kbar (Ferry, 1988b, 1992; Léger and Ferry, 1993). Although we will refer to this dataset as the Silurian-Devonian Waits River and Gile Mountain Formations, two samples in this data set are from the neighboring Albee-Dead River Formation, composed of thinly bedded greenish-grey shale with less common sandstone, which is roughly constrained to between Ordovician and Cambrian in age (Moench et al., 1995). These are biotite zone samples with similar metamorphic histories and P-T conditions as the Gile Mountain Formation nearby (Ferry, 1988b). Numerous studies have been performed on the metamorphism of the region with a focus on fluid infiltration (e.g. Ferry, 1988b; Léger and Ferry, 1993).

A total of 116 samples were utilized in our study from the Waits River, Gile Mountain, and Albee-Dead River Formations—82 metacarbonates, 12 psammites (metamorphosed quartz-rich siliclastics/sandstones), and 20 pelites (metamorphosed fine-grained aluminous siliclastics/claystones)—with mineral assemblages and mineral chemistry from Ferry (1988b), (1992), (1994), (2007), Léger and Ferry (1991), (1993), Penniston-Dorland and Ferry (2006), (2008). Metamorphic grade between carbonate and pelitic isograds was correlated based on temperature estimates; note that the biotite zone in carbonates is approximately the same as the garnet zone (not the biotite zone) in pelites and they have been grouped to prevent confusion.

6.4.1.2 Waterville and Sangerville-Vassalboro Formations, Maine

The Waterville and Sangerville-Vassalboro Formations of Maine record a classic example of the metamorphic gradient following the Buchan series from the chlorite to the sillimanite zone. The Waterville Formation is composed of thinly bedded greenish grey shale, sulfidic black shale, and shaly sandstone with a shaly carbonate member while the overlying Sangerville-Vassalboro Formation is composed of interbedded gray shaly sandstones and carbonates with minor sulfidic black shales (Ferry, 1981, 1983b; Osberg, 1988; Osberg, 1968). Compositional layering occurs on the centimeter to decimeter scale (Ferry, 1981, 1983b). The sequence is dated from Silurian to Devonian based on graptolites within the Waterville and Sangerville-Vassalboro Formations (Osberg, 1968; Pankiwskyj et al., 1976) and subsequent granite intrusions dated at 378 ± 1 to 381 ± 1 Ma (Tucker et al., 2001). The intrusions occurred after structural deformation of the Waterville-Sangerville-Vassalboro Formations, and then the entire package was subjected to regional metamorphism during the Devonian Acadian orogeny, overprinting any contact aureoles (Osberg, 1988; Tucker et al., 2001). Dating on monazite neoblasts in the Waterville Formation suggested that mineral reactions producing andalusite occurred at 364.3 ± 3.5 Ma (Wing et al., 2003). Metamorphic isograds following the Buchan Facies Series have been mapped in the pelitic schists spanning the biotite, garnet, staurolite-andalusite, and sillimanite zones (Osberg, 1968). Isograds in the metacarbonate rocks were also noted from appearances of biotite-chlorite, amphibole-anorthite, zoisite, microcline-amphibole, diopside, and scapolite in increasingly higher grade rocks; these isograds are mapped directly on top of the pelitic isograds so direct comparison is possible (Ferry, 1976b). Numerous studies have highlighted the open system nature of regional metamorphic reactions with fluid infiltration of the rock package (e.g. Ferry, 1988a; Penniston-Dorland and Ferry, 2006). Pressure conditions during metamorphism are estimated at 3.5 kbar with temperature ranging from 380°C at the biotite isograd to 550°C in the sillimanite zone (Ferry, 1976a; Ferry, 1980).

A total of 52 samples were utilized in our study from the Waterville and Sangerville-Vassalboro Formations—35 metacarbonates, 9 psammites, and 8 pelites—with mineral assemblages and mineral chemistry from Ferry (1976b), Ferry (1984), Ferry (1988a), Ferry (1994), and Penniston-Dorland and Ferry (2006). Lithology was poorly denoted within some papers due to analysis of impure carbonates (Ferry, 1976b; Ferry, 1988a), so classification of samples as pelite versus sandstone versus carbonate was made based on the modal volume ratio of micas or carbonates to quartz ($< 25\%$ cut off for pelite or carbonate) and/or the elemental ratio of $\text{Al}_2\text{O}_3/\text{CaO}/\text{SiO}_2$ as per Bickle et al. (1997). Metamorphic grade between carbonate and pelitic isograds was correlated and combined based on the isograd map of the locality from Ferry (1976b) and Ferry (1994) with pelitic schist terminology preferred if there were approximately equivalent metamorphic facies.

6.4.2 Model

For the two targeted localities above, we used the data on iron-bearing minerals to approximate the samples' iron speciation $\text{Fe}_{\text{HR}}/\text{Fe}_{\text{T}}$ and $\text{Fe}_{\text{py}}/\text{Fe}_{\text{HR}}$ ratios, assuming phases were completely and correctly extracted as designed by the standard sequential technique (e.g. Table 6.2). These results were paired with information about the sample lithology and metamorphic zone to understand how progressive metamorphism affects the results of iron speciation. In order to take the published literature data detailed above and use it to find $\text{Fe}_{\text{HR}}/\text{Fe}_{\text{T}}$ and $\text{Fe}_{\text{py}}/\text{Fe}_{\text{HR}}$ ratios, several processing steps were required.

Mineral assemblages are presented in the literature as modal volume percentages or moles per liter rock based on point counting minerals in thin section (usually 2,000 points). For the former, volume percent was converted to molar amount per liter rock using molar volume data from Robie et al. (1967) and Holland and Powell (1998). Hexagonal pyrrhotite's molar volume was used, and molar volumes of micas, garnet, allanite, tourmaline, and amphiboles were found by averaging endmembers. In some trace minerals (less than 0.05 vol%), the

exact abundance of a mineral was not quantified, and simply absence or presence was noted in the published mineral assemblage. If presence was marked, we calculated molar amount per liter rock based on the maximum abundance (0.05 vol%) as well as for the minimal abundance (0 vol%). In various samples, chalcopyrite, pyrite, pyrrhotite, ankerite, calcite, ilmenite, paragonite, muscovite, biotite, chlorite, clinozoisite, allanite, amphibole, staurolite, and tourmaline were listed as trace minerals. Overall, this treatment of trace minerals did not affect the results significantly; however, the change was noticeable in Fe_{py}/Fe_{HR} due to the low abundance of sulfides in many samples (Figs. S6.1-S6.4). All further calculations and discussion in the main text will include the trace minerals and can be treated as a maximum ratio. The amount of iron in the reference 1 liter of rock was calculated by multiplying the moles of a mineral by the iron content within the mineral based on its formula. The mineral formula was calculated based on the published average electron microprobe analyses for each mineral within a given sample/thin section. In some cases, the mineral composition was not precisely published for a given sample. In that case, the average from other samples within the publication at the same metamorphic grade and/or same lithology was used. If this was not possible, the average for the mineral within the publication was used. When no mineral composition data was reported, standard formulas were used and are listed in Table 6.2.

Each mineral was then partitioned into an iron pool following the current standard extraction techniques (Poulton and Canfield, 2005) (Table 6.1): pyrite, carbonate, ferric oxide, magnetite, poorly reactive sheet silicates, or unreactive silicates. The assignments used for all minerals within the model are noted in Table 6.2. Pyrrhotite's assignment was complicated; as discussed above, if studies did not test for pyrrhotite then it would be extracted in Fe_{carb} , but today many studies have started to include a separate extraction test in which case pyrrhotite is grouped with Fe_{py} . In order to have our model comparable to both modern and older iron speciation studies, we have done two sets of calculations with pyrrhotite in either the Fe_{carb} and Fe_{py} pool. After the iron per pool was

summed, non-dimensional ratios of Fe_{py}/Fe_{HR} and Fe_{HR}/Fe_T could be calculated and are presented in Figures 6.3-6.8.

6.5 Case Example Results and Discussion

A wide range of Fe_{py}/Fe_{HR} and Fe_{HR}/Fe_T ratios were found from the data of the Waits River, Gile Mountain, Waterville, and Sangerville-Vassalboro Formations, which would indicate oxic, ferruginous, and euxinic water conditions using the iron speciation proxy (Figs. 6.3, 6.6). We know these samples were deposited in oxic conditions, and there are several factors which could contribute to the high ratios of Fe_{py}/Fe_{HR} and Fe_{HR}/Fe_T . Through more detailed plots to look at trends by lithology and metamorphic zone (Figs. 6.4, 6.5, 6.7, 6.8) as well as the mineral data itself (Figs. 6.9, 6.10), we untangled some of the causes changing Fe_{py}/Fe_{HR} and Fe_{HR}/Fe_T , and discuss the importance of these in actual iron speciation experiments. On a cautionary note, although data were selected carefully to make certain trace minerals were counted, one driver for increased Fe_{py}/Fe_{HR} and Fe_{HR}/Fe_T is simply that iron from certain phases (e.g. oxides or unreactive minerals) was underrepresented by the point counting technique due to small grain size or domains within larger minerals.

6.5.1 Pyrrhotite Pool Placement

One of the largest differences in the ratio results was determined by which pool pyrrhotite was assigned, whether Fe_{carb} or Fe_{py} (Figs. 6.3, 6.6). The Fe_{HR}/Fe_T ratios were not affected since pyrite and carbonate are both highly reactive species and therefore included in Fe_{HR} . However, Fe_{py}/Fe_{HR} was significantly increased due to the additional pyrrhotite fraction in Fe_{py} (Figs. 6.5, 6.8). In the metasedimentary rocks studied here, pyrrhotite in general is more common than other iron sulfides (pyrite or chalcopyrite) across all zones. This addition of pyrrhotite to the Fe_{py} pool was enough to push Fe_{py}/Fe_{HR} ratios above the 0.8 certainty boundary of euxinic redox conditions in some of the carbonates and a sandstone from the Vermont and Maine localities.

Therefore, if pyrrhotite is included in Fe_{carb} as in older studies or through misdiagnosis of the mineral assemblage, the samples will appear much more ferruginous than paleoredox conditions, assuming that the iron in the pyrrhotite comes from the metamorphic transformation of water-column pyrite or primary precipitation. In fact, prior metamorphic analyses on pelites from the Waterville Formation suggested a direct transformation of iron in pyrrhotite into pyrite due to a progressive loss of sulfur (Ferry, 1981). On the other hand, pyrrhotite can form from the decomposition of iron oxides and iron silicates even at low-metamorphic grade ($<200^{\circ}C$) with addition of H_2S fluids or co-decomposition of pyrite (Gillett, 2003; Hall, 1986; Nesbitt and Kelly, 1980; Tracy and Robinson, 1988). In these circumstances, placing pyrrhotite in the Fe_{py} pool is erroneous and will drive rocks toward the euxinic zone giving poor paleoenvironmental interpretations. Careful petrographic study of the pyrrhotite could help determine which scenario is the case through pseudomorphs, rims, or partially reacted phases (e.g. Zhou et al., 1995). Isotope study could help determine the importance of S-rich fluids (e.g. Gillett, 2003), although determining “background” or “normal” could be difficult in ancient, relatively metamorphosed samples. Mineral assemblages could give clues as well, but often clear-cut metamorphic grades cannot be or are not sampled. The simplest solution is to avoid analysis of samples containing pyrrhotite.

6.5.2 Lithological Controls and Diagenesis

Another striking variable which appears to be an important control on iron speciation ratios is the lithology of the samples. To a certain degree, different lithologies should represent different paleoenvironments, e.g. sandstones are nearer to shore with more detrital inputs and shallower waters than shales and carbonates (Walker and James, 1992). However, fine-scale interbedding is noticed within all of the formations studied here, and within the Waterville and Gile Mountain Formations, it is clearly detailed that these thin interbeds of carbonates, pelites, and psammites were sampled (e.g. Ferry, 1994). Additionally,

we understand that all results should show oxic water column conditions based on the global biological constraints of aerobic benthic animals, and therefore high Fe_{HR}/Fe_T or Fe_{py}/Fe_{HR} values implying ferruginous or euxinic conditions should be investigated.

Lithological differences were most noticeable in Fe_{HR}/Fe_T , where pelites had much lower values and a lower range than psammites and carbonates of the same formation regardless of metamorphic zone (Figs. 6.4a, 6.7a). Even if samples only were examined at the lowest metamorphic grades (chlorite, ankerite, biotite) to separate that confounding factor, pelites had low Fe_{HR}/Fe_T ratios compared to the carbonates and psammites at the same metamorphic grade (Figs. 6.4bcd, 6.7bcd.) Additionally, at low-metamorphic grades, Fe_{py}/Fe_{HR} was generally higher in pelites than in psammites and carbonates (Figs. 6.5bcd, 6.8bcd), especially when pyrrhotite was included in the Fe_{py} pool (Figs. 6.5fgh, 6.8fgh).

By looking at the mineralogy/detailed calculations, it became clear that the primary reason for the differences between lithologies was the abundance of iron in carbonates either as minor components in calcite or as ankerite (Figs. 6.9d, 6.10d). Almost all of the psammites studied here included some carbonate minerals while the pelites had much lower amounts of carbonate. Although previous geochemical work suggested that carbonate samples behave in the Fe_{HR}/Fe_T proxy similarly to siliciclastic samples (Clarkson et al., 2014), this work was performed on modern carbonates with minimal diagenetic overprints. Iron can be incorporated into carbonates in primary precipitates; however, in modern oxygenated waters, soluble iron contents are very low, so most iron is incorporated in carbonates through early or secondary diagenetic cements formed in anoxic pore fluids (Barnaby and Rimstidt, 1989; French, 1973; Warren, 2000). As shown here, these diagenetic overprints could dominate the Fe_{HR}/Fe_T signals in Paleozoic carbonate rocks enough to create erroneous paleoredox interpretations for the water column. Notably, this signal was not simply due to the presence of ankerite in samples, which has been suggested as a screening method for

diagenetic alteration before doing iron speciation (Clarkson et al., 2014). Trace amount of iron in calcite constituted over 50% of the Fe_{carb} pool in almost all of the low-grade carbonates and even samples with low abundances of ankerite had high Fe_{HR}/Fe_T above the boundaries of the anoxic zone. In contrast, more of the iron in the Fe_{carb} pool of low-grade psammities usually came from ankerite, and its presence in siliciclastics could be a better signal for diagenetic alteration. Overall, samples with proportionately large Fe_{carb} pools should be investigated petrographically to determine whether the carbonates are primary or not. Calibration of the Fe_{HR}/Fe_T ratios on modern samples (and without the new sequential extraction system) ignores this important pool of diagenetic transformations, which will affect the proxy.

The observation that low-grade pelites had higher Fe_{py}/Fe_{HR} ratios than psammities or carbonates was also expected from common early diagenetic reactions. Although pyrite can form within the water column (Raiswell and Berner, 1985; Wilkin and Barnes, 1997), it also forms in sediments underlying oxic and sub-oxic waters through scavenging of highly-reactive iron in pore waters that are anoxic and sulfide-rich (Berner, 1970; Canfield and Berner, 1987; Wilkin et al., 1996). Due to their high organic content and slow depositional rate, deep-water shales are more likely to form pyrite than sandstones or carbonates (e.g. Berner, 1984; Curtis, 1978). Although low-grade pelites had higher Fe_{py}/Fe_{HR} ratios than other lithologies, generally these higher ratios were not large enough to fall within the boundaries for euxinic conditions, suggesting the proxy is less sensitive to diagenetic alteration. Notably, the pelite data used in this study had approximately 1 vol% sulfides with one sample in the Waterville Formation containing 3.2 vol% sulfides. Within the Waits River, Waterville, and Sangerville-Vassalboro Formations, there are distinct sulfidic black shale layers containing over 10 vol. % sulfides (Waterville Formation, Ferry, 1981) that are closer to the expected facies for a euxinic water column-system.

6.5.3 Increasing Grade and Metamorphic Reactions

The detailed breakdown of the Fe_{HR}/Fe_T and Fe_{py}/Fe_{HR} ratios by metamorphic zone highlighted trends that occur with increasing metamorphic grade (Figs. 6.4, 6.5, 6.7, 6.8). Observations of trends were clearer in the Waits River and Gile Mountain Formation due to the larger number of data points, but the Waterville and Sangerville-Vassalboro samples were also considered in untangling these numerical shifts and their causes. Fe_{HR}/Fe_T in general decreased with increasing grade, although slight differences were seen between the siliciclastic and carbonate samples (Figs. 6.4bcd, 6.7bcd). While a more monotonic decrease was seen in siliciclastics starting from the chlorite zone, the decrease in carbonates occurred only after the garnet zone. The kyanite zone carbonates of the Waits River with the highest P-T conditions in either locality (Ferry, 1994; Penniston-Dorland and Ferry, 2006) showed a sudden return to previous values.

Fe_{py}/Fe_{HR} was more complicated, but it appears metamorphic effects are separated by lithology. In pelitic samples, the Fe_{py} pool was differently affected based on the inclusion or exclusion of pyrrhotite. When pyrrhotite was excluded from the Fe_{py} pool, a slight increase in Fe_{py}/Fe_{HR} occurred with metamorphic grade whereas when pyrrhotite was included in the Fe_{py} pool, a decrease was observed. (Note: the Waterville Formation staurolite zone sample is probably an outlier due to lithological differences; it contains the 3.2 vol% pyrrhotite discussed earlier.) In carbonate samples, trends were difficult to resolve when pyrrhotite was excluded from the Fe_{py} pool due to distinct variable directional shifts in the Vermont and Maine localities. We chose not to make further observations due to concerns of over-interpreting a single point's importance or small magnitude complex trends. However, when pyrrhotite was included in the Fe_{py} pool, values for Fe_{py}/Fe_{HR} for carbonates increased with increasing metamorphic grade with some samples falling within the limits for euxinic redox conditions at high grades. Notably, the highest-grade samples from the kyanite and scapolite zones showed a decrease in Fe_{py}/Fe_{HR} similar to the rebound seen in Fe_{HR}/Fe_T in this metamorphic zone. Psammite samples were the least numerous

in these studies; no clear trend appeared in either of the localities, although the three high Fe_{py}/Fe_{HR} ratios within the euxinic boundaries occurred in samples from above the biotite isograd.

It was clear that these ratio changes of Fe_{HR}/Fe_T and Fe_{py}/Fe_{HR} were due to movement of iron between different pools during progressive metamorphism; however, for each ratio, we needed to determine which of the two pools was changing in size (or whether both were changing). Total iron did not vary systematically with metamorphic grade, although it did by lithology (Figs. 6.9a, 6.10a), suggesting that these metamorphic systems were closed with respect to iron although open with respect to fluids carrying C-O-H-S and other elements (e.g. Ferry, 1981, 1983b, 1988b). Therefore, the individual pools were normalized by total iron for comparison purposes. Additionally, changes in Fe_{carb} , Fe_{mag} , Fe_{py} , Fe_{PRS} , and Fe_U could occur due to changes in abundances of minerals or due to changes in mineral composition with loss or addition of iron; we did not distinguish between these options, although in general it appears that abundance plays a larger role since Fe compositions of minerals did not vary greatly across metamorphic zones (at least within the publications). The one possible exception is ankerite, which on average may lose iron with increasing metamorphic grade (e.g. Waits River Formation, Ferry (1992) and Waterville Formation, Ferry (1994)), but this trend did not reproduce well in all studies.

For Fe_{HR}/Fe_T , the main driver appeared to be variation in the Fe_{carb} pool, specifically of the iron carbonates, not pyrrhotite. In carbonate samples, a decrease in Fe_{carb} began within the garnet zone for a significant drop afterwards with an upswing at the kyanite zone while in pelites and psammites, a sharp decrease occurred after the biotite zone and continued slowly with increasing metamorphic grade (Figs. 6.9d, 6.10d). There was an inverse correlation with these decreases and increases in the Fe_U pool suggesting that the metamorphic formation of silicates containing iron such as garnet, amphibole, etc. utilized iron from iron carbonates (Figs. 6.9b, 6.10b). Although Fe_{PRS} was at times a significant part of the total iron pool, the poorly reactive sheet silicates did not

appear to drive Fe_{HR} or Fe_T to any substantial degree and the data from the two localities differ greatly. In the Waterville and Sangerville-Vassalboro Formations, significant formation of sheet silicates was seen in carbonate samples in the biotite and garnet zone with subsequent destruction; with a lack of samples in sub-biotite zones, siliciclastic rocks simply showed progressive decrease of Fe_{PRS} after the biotite zone (Figs. 6.10ef). In the Waits River and Gile Mountain Formations, no significant trends in sheet silicates were seen within pelites and psammities whereas the carbonate samples showed a significant increase in Fe_{PRS} in the garnet zone, which is correlative to the biotite zone in carbonates and thus not unexpected (Figs. 6.9ef). Although a decrease in Fe_{PRS} was seen within the diopside zone, there was a return to high values in the kyanite zone so distinctions in lithological sampling could be biasing the diopside results. Metamorphically, this suggests that several reactions exist forming and destroying micas and chlorite across metamorphic grades or that multiple minerals are involved in reactions adding complexity; within carbonates, iron may come from iron carbonates for the formation of biotite and transfer upon destruction to help form unreactive silicates (or pyrrhotite) while siliciclastic rocks may have more internal cycling of iron within the Fe_{PRS} pool. It is interesting that some of the iron transitions are fairly abrupt whereas others, such as the slow decrease in biotite with metamorphic grade, occur progressively across increasing metamorphic regimes.

Fe_{mag} only contained ilmenite in this study and overall is a relatively small amount of the Fe_T pool especially in carbonates. Therefore, changes in ilmenite did not significantly affect the Fe_{HR}/Fe_T ratios, but did show interesting trends with metamorphic implications. In carbonate samples, ilmenite showed significant increases at the garnet zone whereas in pelites, ilmenite decreased across increasing metamorphic grades (Figs. 6.9c, 6.10c). Psammities appeared to be a mixture of these changes with a slight decrease until the kyanite zone where Fe_{mag}/Fe_T ratios return to their former values. From the literature, it is unclear whether the iron in ilmenite is actually “highly reactive” toward sulfides; it is

included in Fe_{mag} due to sequential extraction methodology studies. Within carbonates, ilmenite varied similarly to unreactive silicate phases, while in pelites, it appeared to be transformed slowly through metamorphism.

Deconvolving causes of the Fe_{py}/Fe_{HR} trends was more difficult due to less clear variations, low abundance of iron sulfides, and the large changes in Fe_{HR} detailed above. In the pelites, chalcopyrite and pyrite did not change in fraction very much across metamorphic zones; slight increases in Fe_{py}/Fe_{HR} when pyrrhotite was in the Fe_{carb} pool appeared to be related to decreases in the rest of the Fe_{HR} pools. Pyrrhotite did significantly decrease in pelites after the biotite zone, which drove the decreases in Fe_{py}/Fe_{HR} when pyrrhotite was in the Fe_{py} pool. For carbonates, pyrrhotite might increase slightly with metamorphic grade (on average), which combined with the decrease of the Fe_{HR} pool increased the Fe_{py}/Fe_{HR} ratio. Based on detailed analysis of the raw data, pyrrhotite formation might also be dependent on lithological differences or local fluid flow conditions as certain sites had higher pyrrhotite abundances than other sites at the same metamorphic grade. Although this is a factor to consider in all the mineralogical changes discussed above, the low amount of sulfides highlighted this variability in pyrrhotite abundance.

The trends and shifts described above correspond to metamorphic reactions known to occur with increasing pressure and temperature. Prior work on the Waits River, Gile Mountain, Waterville, and Sangerville-Vassalboro Formations has proposed various metamorphic reactions based on analysis of mineral assemblages and thermodynamic calculations, which correspond well to the changes seen above (Table 6.3). However, prior studies usually did not focus on the iron mineralogy, sometimes excluding iron or accessory minerals entirely from calculations, so some transformations were not accounted for but are well known from other sites (Table 6.3). We display these metamorphic reactions by metamorphic grade as well as others, which may not have occurred in the Paleozoic sediments of the eastern US, in iron speciation space to elucidate the potential effects of iron mobility during metamorphism on the iron speciation

redox proxy (Fig. 6.11). Notably, some of the phases affecting the iron speciation ratios in the data-driven model above (including important factors like calcite) do not contain Fe in their general formulas/endmember stoichiometries (Table 6.2) expanding the number of metamorphic reactions that could affect iron systematics significantly.

6.6 Conclusions

Iron speciation is a widely used proxy for understanding paleoredox of ancient oceans and lakes; however, it is empirically calibrated on modern sediments and errors could occur through improper boundaries for interpreted redox conditions, mixing of iron between pools in sequential extraction, or due to diagenetic and metamorphic transformations. Utilizing data from the metamorphic petrology literature of sedimentary strata deposited in Paleozoic oxic marine conditions, we assessed how variations in metamorphic grade, lithology, and iron speciation pool placement (through different extraction techniques) affect the iron speciation proxy.

Pyrrhotite and iron in carbonates stood out as important minerals affecting the proxy for our data set. Grouping pyrrhotite in the Fe_{carb} pool (as in older studies or those that do not screen for pyrrhotite) provided significantly lower estimates of Fe_{py}/Fe_{HR} than when it was grouped with the sulfides in Fe_{py} . The correct pool will vary based on the locality, lithology, and metamorphic reactions. Although study of low-grade pelites suggested the pyrrhotite in our samples formed from pyrite and should be grouped in the Fe_{py} pool (Ferry 1981), pyrrhotite did appear to be added to the carbonate rocks during progressive metamorphism with minimal decrease in pyrite suggesting iron movement from other pools. Iron carbonates were prevalent across all three types of lithologies and significantly increased the Fe_{HR}/Fe_T ratios suggesting ferruginous depositional conditions. In fact, these carbonates probably formed in anoxic pore fluids in early or late diagenetic processes and do not reflect water column chemistry. With increasing metamorphic grade, the iron within this carbonate transferred to

the silicate pool ($\text{Fe}_{\text{PRS}} + \text{Fe}_{\text{U}}$) and significantly decreased the $\text{Fe}_{\text{HR}}/\text{Fe}_{\text{T}}$, which could be an erroneous oxic result if an anoxic water column did exist during deposition. Proportionately less carbonate was seen within the pelitic samples and even through increasing metamorphic grade, this lithology preserved the oxic paleoredox information better than psammites and carbonate samples. Overall, the iron speciation proxy is heavily affected by early diagenetic minerals and secondary diagenetic/metamorphic reactions especially in carbonate lithologies.

Plotting iron data from sedimentary rocks within iron speciation space also provided a new perspective to analyze the mobility of iron during progressive metamorphism. Iron moved from iron carbonates to form poorly reactive sheet silicates and unreactive silicate minerals in the biotite, garnet, and amphibole zones. Biotite formation within carbonates occurred in the pelitic schist garnet zone, and by delaying this metamorphic reaction, the formation of unreactive silicates started mainly in the amphibole zone. In carbonates, ilmenite formed at the same time as these unreactive silicates whereas in pelites and psammites, ilmenite acted as a reactive oxide phase that was slowly consumed. In pelites, pyrrhotite was also destroyed through progressive desulfurization reactions with increasing grade, but in carbonates a slight increase in abundance occurred, suggesting the iron for its formation could come from the iron carbonate pool. Many of these reactions have been previously hypothesized by study of metamorphic mineral assemblages, and our work provides corroboration while highlighting the mobile nature of iron in diagenesis and metamorphism. A unit of rock may encounter several redox environments over the course of its history, and untangling these environments to understand paleoredox and sustainability for life requires the application of multiple techniques, specifically textural analyses.

6.7 Acknowledgements

Support for this work was provided by the NSF Graduate Research Fellowship program (S.P.S.) and NASA Earth and Space Fellowship (S.P.S.).

6.8 Tables

Table 6.1: Sequential extraction methods and targeted minerals

Pool	Short Name*	Details	Extractable Fe from Minerals †	Source§
Fe _{carb}	Acetate	(1) 1M Na Acetate, pH 4.5, 24 hours room temperature or 48 hours 50°C	Carbonate iron, siderite, ankerite (pyrrhotite)	1
Fe _{ox1}	Hydroxylamine	(2) 1M Hydroxylamine-HCl, 48h	Ferrihydrite, lepidocrocite	1
Fe _{ox2}	Dithionite	(3) Na dithionite solution (50 g l ⁻¹), pH 4.8, 2 hours	Goethite, akaganéite, hematite (ferrihydrite, lepidocrocite)	1
Fe _{mag}	Oxalate	(4) 0.2 M ammonium oxalate/0.17 M oxalic acid, pH 3.2, 6 hours	Magnetite (titanomagnetite, ilmenite, goethite, ferrihydrite, lepidocrocite, siderite, pyrrhotite)	1,2,3,4
Fe _{PRS}	Boiling HCl	(5) 12 M HCl, 1 minute boiling	Poorly reactive sheet silicates like nontronite, biotite, chlorite, glauconite (all of the above)	1, 5
Fe _{py}	CRS	Chromium reduction with 1 M CrCl ₂ solution, 2 hours boiling + Zn, Ag distillation	Pyrite (pyrrhotite, S, Ni-Zn-Cu-As-Cd-Pb sulfides)	1,6,7
Fe _U	--	Total iron (from XRF, ashing and boiling in 6 M HCl, etc.) minus above sum	Silicates	1
--	AVS	Several options using HCl of different strengths, temperatures, times ± chlorides	Monosulfides like amorphous FeS, mackinawite, greigite, pyrrhotite	8,9

* Abbreviations: CRS = chromium-reducible sulfide, AVS = acid-volatile sulfide

† Minerals in parenthesis are those that can be extracted in this step, but should already have been extracted using the sequential extraction technique or are not the targeted minerals.

§ References: 1) Poulton and Canfield (2005), 2) Dold (2003), 3) Algoe et al. (2012), 4) Burton et al. (2006), 5) Raiswell et al. (1994), 6) Canfield et al. (1986), 7) Schumann et al. (2012), 8) Cornwell and Morse (1987), 9) Praharaj and Fortin (2004)

Table 6.2: Minerals identified within the Waits River, Gile Mountain, Waterville, and Sangerville-Vassalboro Formations

Name	General Formula	Assumed Formula	Assigned Iron Pool
Fe-bearing minerals			
Muscovite	$KAl_2(AlSi_3O_{10})(OH)_2$	--	Fe _{PRS}
Paragonite	$NaAl_2(AlSi_3O_{10})(OH)_2$	--	Fe _{PRS}
Biotite	$K(Mg,Fe)_3(AlSi_3O_{10})(F,OH)_2$	--	Fe _{PRS}
Chlorite	$(Al,Fe, Mg, Mn, Ti)_{5-6}(Al,Fe, Si)_4(O, OH)_{18}$	--	Fe _{PRS}
Calcite	$CaCO_3$	--	Fe _{carb}
Ankerite	$Ca(Fe, Mg, Mn)(CO_3)_2$	$CaFe_{0.5}Mg_{0.5}(CO_3)_2^*$	Fe _{carb}
Ilmenite	$FeTiO_3$	$FeTiO_3^\dagger$	Fe _{mag}
Pyrrhotite	$Fe_{(1-x)}S$ (x = 0 to 0.2)	$Fe_{0.95}S$ or $Fe_{0.907}S$ §	Fe _{carb} or Fe _{py}
Pyrite	FeS_2	FeS_2	Fe _{py}
Chalcopyrite	$CuFeS_2$	$CuFeS_2$	Fe _{py}
Epidote	$Ca_2Al_2Fe(Si_2O_7)(SiO_4)O(OH)$	--	Fe _U
Allanite	$(Ce, Ca, Y, La, etc.)_2(Al, Fe)_3(SiO_4)_3(OH)$	$CeCaFe_{1.5}Al_{1.5}(SiO_4)_3(OH)$	Fe _U
Clinozoisite-Zoisite	$Ca_2Al_3(Si_2O_7)(SiO_4)O(OH)$	--	Fe _U
Garnet	$(Ca, Mg, etc.)_3(Fe, Al, Ti, etc.)_2(SiO_4)_3$	--	Fe _U
Staurolite	$Fe_2Al_9Si_4O_{23}(OH)$	$Fe_2Al_9Si_4O_{23}(OH)^\#$	Fe _U
Diopside	$CaMgSi_2O_6$	--	Fe _U
Amphibole	$(Na, K, Ca, Pb, \square)(Li, Na, Mg, Fe, Mn, Ca)_2$ $(Li, Na, Mg, Fe, Mn, Zn, etc.)_5(Si, Al, Ti)_8O_{22}$ $(OH, F, Cl, O)_2^{**}$	--	Fe _U
Tourmaline	$(Ca, Na, K, \square)(Al, Fe, Li, Mg, Mn)_3(Al, Cr, Fe, V)_6$ $Si_6O_{18}(BO_3)_3(O, OH)_3(F, O, OH)^{**}$	$NaFeMg_2Al_6(Si_6O_{18})(BO_3)_3$ $(OH)_3(OH)$	Fe _U
Non-Fe bearing minerals			
Quartz	SiO_2	--	--
Plagioclase	$NaAlSi_3O_8 - CaAl_2Si_2O_8$	--	--
Titanite	$CaTi(SiO_4)O$	--	--
Rutile	TiO_2	--	--
Graphite	C	--	--
Alkali feldspar	$KAlSi_3O_8$	--	--
Kyanite	$Al_2(SiO_4)O$	--	--
Apatite	$Ca_5(PO_4)_3(F, Cl, OH)$	--	--
Zircon	$Zr(SiO_4)$	--	--
Monazite	$(Ce, La, Nd, Th, Sm, Gd)PO_4$	--	--
Scapolite	$Na_4Al_3Si_9O_{24}Cl - Ca_4Al_6Si_6O_{24}CO_3$	--	--
* Assumed formula only used for trace amounts in Léger and Ferry (1991).			
† Assumed formula is used in all studies except Gile Mountain and Waits River Formation data from Ferry (1994) and Ferry (2007).			
§ $Fe_{0.95}S$ was used as the assumed formula for the Waits River and Gile Mountain Formation samples. $Fe_{0.907}S$ was used as the assumed formula for the Waterville and Sangerville-Vassalboro Formation samples since this is the average pyrrhotite composition from 18 samples in the Waterville Formation (Ferry, 1981).			
# Assumed formula only used for trace amounts in Ferry (1994).			
** \square stands for no element in this structural position.			

Table 6.3: Example metamorphic reactions that transfer iron between pools*

Eq.	Equation†	Lithology	Locality or Model-System§	Zone	Ref.#
1	2 py + CH ₄ → 2 po + 2H ₂ S + C	Graphitic pelite	Waterville	<chlorite	1
2	2.689 ms + 4.648 pl + 1.99 qz + 1.567 dol + 0.029 po + 0.03 rt + 3.139 CH ₄ → bt + 6.269 pl + 1.6 afs + 6.273 C + 0.029 H ₂ S + 7.937 H ₂ O	Graphitic pelite	Waterville	biotite	1
3	ms + 3 qz + 8 ank + 4 H ₂ O → 8 cal + chl + bt + 8 CO ₂	Calcareous pelite	Waterville & Sangerville-Vassalboro	biotite	2
4	5 ms + 8 cal + 3 chl + 7 qz → 5 bt + 8 pl + 12 H ₂ O + 8 CO ₂	Calcareous pelite	Waterville & Sangerville-Vassalboro	biotite	2
5	2.77 ms + 0.26 ilm + 11.04 ank + 1.86 qz + 4.02 H ₂ O + 0.08 HCl → chl + 2.83 bt + 11.87 cal + 10.21 CO ₂ + 0.08 NaCl	Carbonate	Sangerville-Vassalboro	biotite	3
6	0.98 ms + 2.23 ank + 0.65 qz + 0.09 ilm + 0.03 HCl + 0.01 H ₂ O → 1.09 bt + 1.89 cal + 0.48 pl + 0.03 NaCl + 2.57 CO ₂	Carbonate	Sangerville-Vassalboro	biotite	3
7	ms + 1.28 cal + 0.84 HCl → 0.12 bt + 0.02 spn + 0.36 qz + 1.22 pl + 0.79 KCl + 0.05 NaCl + 1.30 H ₂ O + 1.28 CO ₂	Carbonate	Sangerville-Vassalboro	biotite	3
8	ilm + 2 cal + qz → spn + ank	Carbonate	Sangerville-Vassalboro	biotite	4
9	afs + 3po + 4H ₂ O → bt + 3 H ₂ S	Graphitic pelite	Waterville	garnet	1
10	0.560 ms + 0.174 chl + 1.080 cal + 0.006 ilm + 0.953 HCl → 0.190 bt + 0.173 grt + 0.394 pl + 0.941 qz + 1.080 CO ₂ + 1.541 H ₂ O + 0.621 NaCl + 0.332 KCl	Carbonate	Waterville	garnet	5
11	5 ank + 8 qz + H ₂ O → amp + cal + 7 CO ₂	Carbonate	Waterville	garnet	6
12	chl + 2.94 cal + 5.73 qz + 0.05 ilm + 0.19 pl → 1.02 amp + 0.86 pl + 2.94 CO ₂ + 2.98 H ₂ O	Carbonate	Sangerville-Vassalboro	amphibole	3
13	0.07 amp + 0.59 cal + 1.31 pl + 0.01 HCl + 0.59 H ₂ O → zois + 0.002 spn + 0.10 qz + 0.01 NaCl + 0.59 CO ₂ + 0.16 H ₂	Carbonate	Sangerville-Vassalboro	zoisite	3
14	2 py + H ₂ O + C → 2 po + 2 H ₂ S + CO ₂	Graphitic pelite	Waterville	sillimanite	1
15	1.378 ms + 0.049 chl + 0.33 qz + 0.485 ank + 2.641 sd + 0.340 rt → 1.492 bt + 0.454 pl + 0.254 ilm + 3.162 CO ₂ + 0.082 H ₂	Pelite	Gile Mountain	biotite	7

Table 6.3 (continued)

Eq.	Equation†	Lithology	Locality or Model-System§	Zone	Ref.#
16	0.005 ms + 0.052 ank + 0.056 pl + 0.002 rt + 0.068 CO ₂ --> 0.172 cal + 0.25 qz + 0.005 H ₂ O	Carbonate	Gile Mountain	biotite	7
17	1.021 ms + 0.034 chl + 1.497 ank + 0.024 rt + 1.573 HCl --> 0.465 bt + 0.225 pl + 0.324 grt + 1.579 qz + 2.994 CO ₂ + 1.479 H ₂ O + 1.139 NaCl + 0.434 KCl	Psammite	Gile Mountain	garnet	5
18	0.007 bt + 0.119 chl + 0.065 ank + 0.078 pl + 0.279 qz --> 0.003 ms + 0.252 grt + 0.002 ilm + 0.129 CO ₂ + 0.481 H ₂ O	Pelite	Waits River	garnet	5
19	ilm + py --> 2 po + rt + 0.5 O ₂	Graphitic pelite	FTS-GCOHS	<chlorite	8
20	4 py + 3 CO ₂ + CH ₄ + H ₂ O --> 4 sd + 8 H ₂ S	Graphitic pelite	NCKFMASH-S	chlorite	9
21	chl + 4 hem --> cld + 4 mag + 2 qz + H ₂ O	Fe-rich pelite	FASH	chlorite	10
22	3 chl --> 3 alm + 2 mag + 12 H ₂ O (+ QFM)	Fe-rich pelite	FASH	garnet	10
23	mag + 3 py + 2 C --> 6 po + 2 CO ₂	Carbonate	Orr Fm., UT	<chlorite	11
24	3 sid + 0.5 O ₂ --> mag + 3 CO ₂	Iron formation	Biwabik Fm., MN & Naugeene Fm., MI	chlorite	12,13
25	5.31 ank + 8.75 pg + 4.8 po + 3.57 pl + 16.83 qz + 1.97 O ₂ --> grt + 16.44 pl + 1.53 chl + 2.4 S ₂ + 1.9 H ₂ O + 10.62 CO ₂	Pelite	Horsethief Creek Grp., British Columbia	garnet	14
26	bt + 3 py + 1.5 CH ₄ --> afs + 6 po + 4 H ₂ O + 1.5 C	Graphitic pelite	Partridge and Paxton Fm., MA	sillimanite	15
27	ilm + H ₂ S --> rt + po + H ₂ O	Graphitic pelite	Partridge and Paxton Fm., MA	sillimanite	15
28	bt + 3 H ₂ S --> afs + 3 po + 4 H ₂ O	Graphitic pelite	Partridge and Paxton Fm., MA	sillimanite	15
29	2 ank + 3 qz --> di + opx + cal + 3 CO ₂	Iron formation	Wabush Fm., Newfoundland	kyanite	16
30	14 ank + 16 qz + H ₂ O --> tr + amp + 14 cal + 14 CO ₂	Iron formation	Wabush Fm., Newfoundland	kyanite	16

* The numerous reactions moving iron between poorly reactive silicate and unreactive silicate pools are not included in this sampling.

† Abbreviations for minerals following Whitney and Evans (2010)

§ Abbreviations: N = Na₂O, C = CaO, K = K₂O, F = FeO, M = MgO, T = TiO₂, S = SiO₂, A = Al₂O₃, H = H₂O, -GCOHS = graphite saturated C-O-H-S fluids, -S = H₂S, Fm. = Formation, Grp. = Group, UT = Utah, MN = Minnesota, MI = Michigan, MA = Massachusetts

References: 1) Ferry (1981), 2) Ferry (1976b), 3) Ferry (1983a), 4) Ferry (1983b), 5) Ferry (1994), 6) Ferry (1979), 7) Ferry (1988b), 8) Connolly and Cesare (1993), 9) Tomkins (2010), 10) Bucher and Frey (2002), 11) Gillett (2003), 12) Jones (1972), 13) French (1973), 14) Haase (1982), 15) Tracy and Robinson (1988), 16) Klein (1966)

6.9 Figures

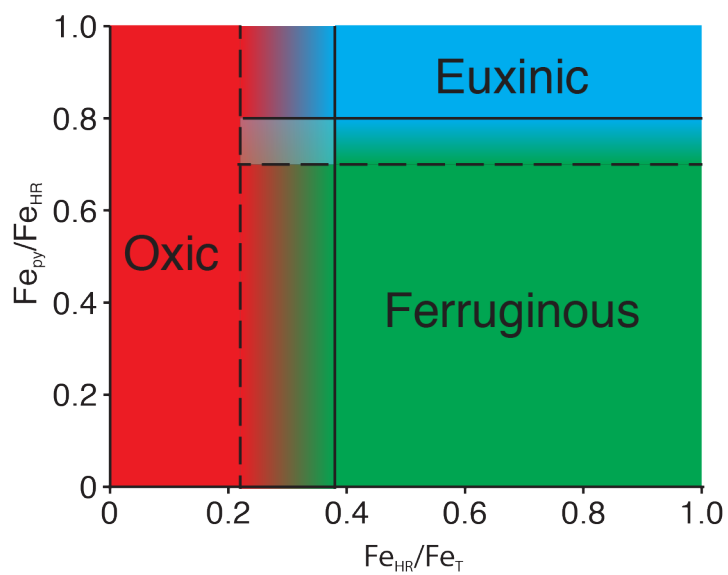


Figure 6.1: Iron Speciation cross-plot with ratio of pyrite iron to highly reactive iron (Fe_{py}/Fe_{HR}) plotted against highly reactive iron to total iron (Fe_{HR}/Fe_T) with paleowater column redox conditions bounded by limits from empirical calibrations discussed in text.

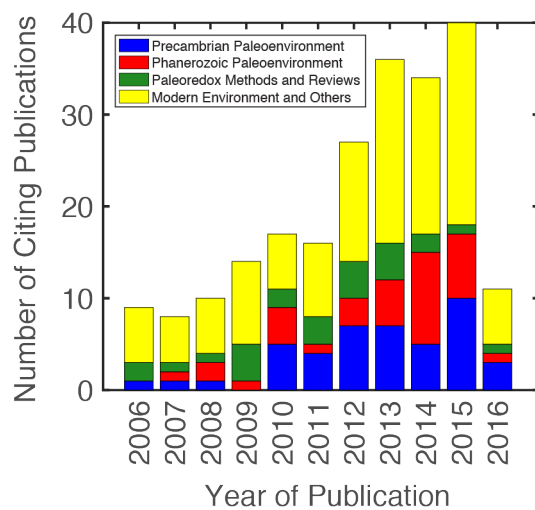


Figure 6.2: Stacked bar graph showing widespread use and growing popularity of iron speciation technique as a paleoenvironmental redox proxy based on number of publications each year citing the sequential extraction methods paper (Poulton and Canfield, 2005). Total number of citations is 222; data from Web of Science citation report accessed April 25, 2016.

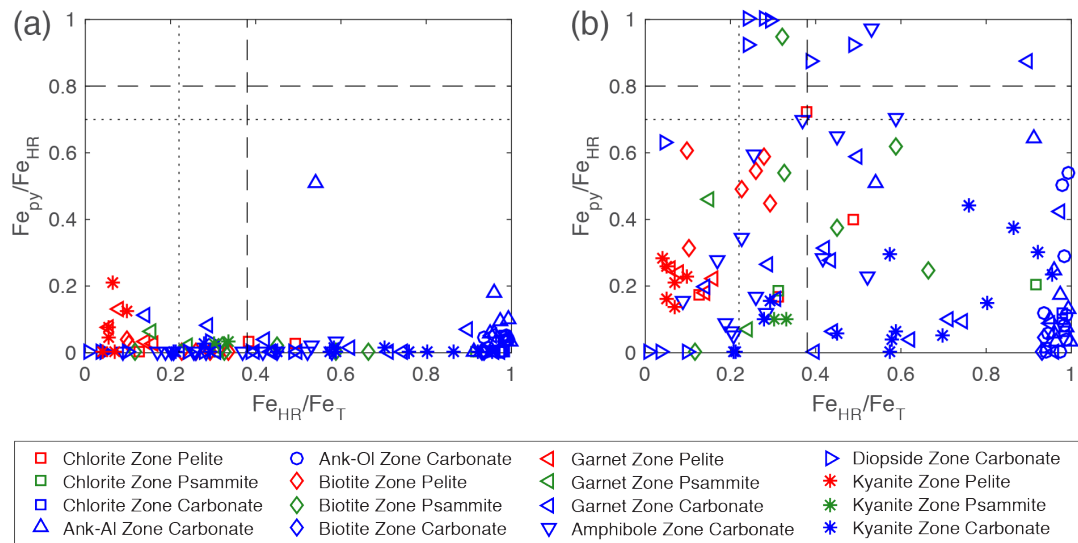


Figure 6.3: Waits River and Gile Mountain Formation data plotted in iron speciation space. Legend is the same for both plots with different symbols representing the 8 different metamorphic zones color-coded by lithology. Ank-Al stands for Ankerite-Albite and Ank-Ol stands for Ankerite-Oligoclase. (a) Pyrrhotite in the iron carbonate (Fe_{carb}) pool. (b) Pyrrhotite in the pyrite pool (Fe_{py}). Fe_{py}/Fe_{HR} is the ratio of pyrite to highly reactive iron and Fe_{HR}/Fe_T is the ratio of highly reactive to total iron. Figures 6.4 and 6.5 show expanded plots for more detail.

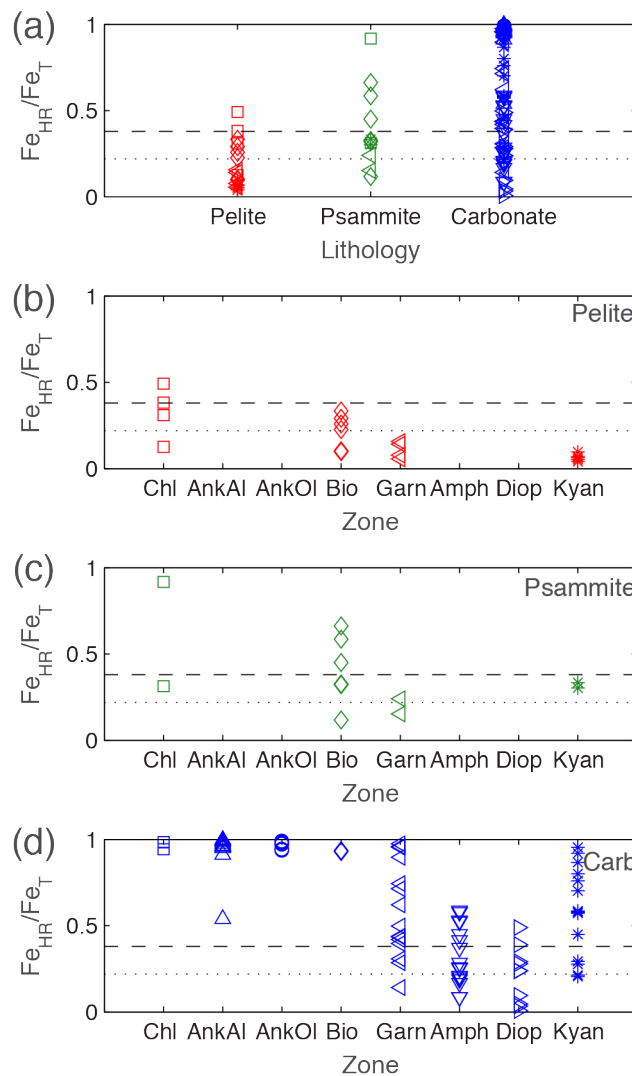


Figure 6.4: Highly reactive iron to total iron (Fe_{HR}/Fe_T) ratios in detail separated by lithology and zone for Waits River and Gile Mountain Formations. Same symbols as Figure 6.3; here labeled on the plots with symbols for metamorphic zone color-coded by lithology. Abbreviations are: Chl = Chlorite, Ank-Al = Ankerite-Albite, Ank-Ol = Ankerite-Oligoclase, Bio = Biotite, Amph = Amphibole, Diop = Diopside, Kyan = Kyanite, Carb = Carbonate.

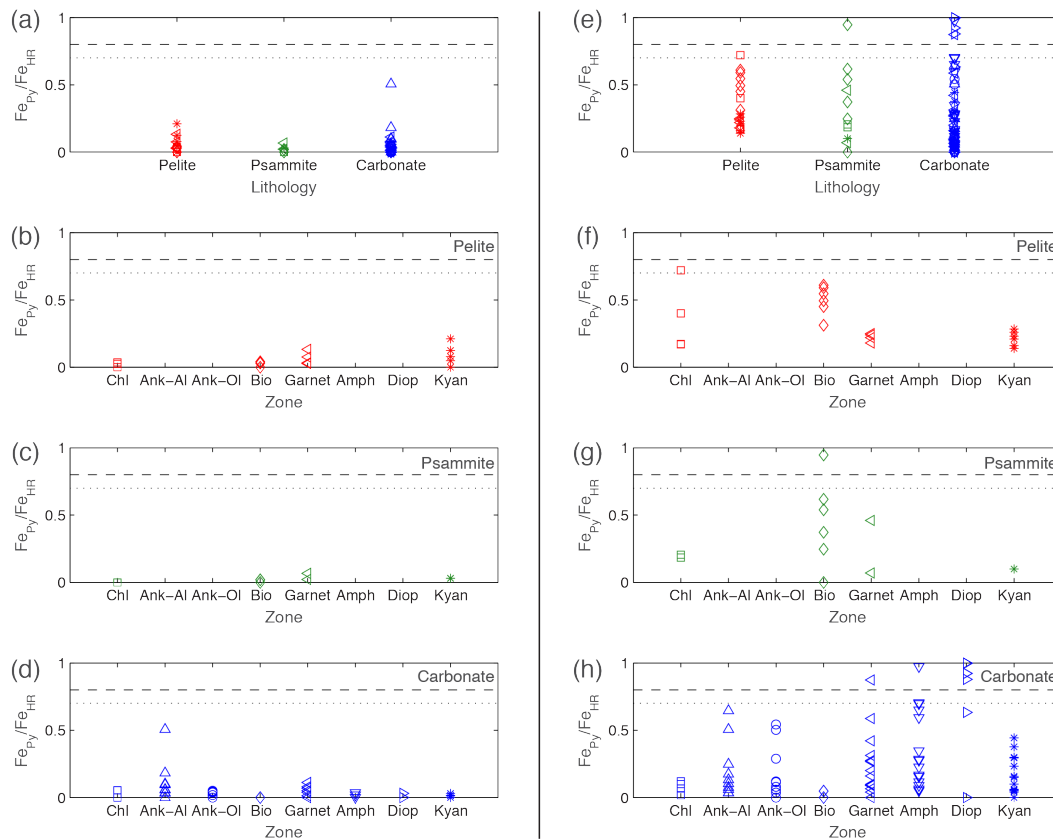


Figure 6.5: Pyrite to highly reactive iron (Fe_{py}/Fe_{HR}) ratios in detail separated by lithology and zone for Waits River and Gile Mountain Formations. (a-d) Pyrrhotite in the iron carbonate (Fe_{carb}) pool. (e-h) Pyrrhotite in the Fe_{py} pool. Same symbols as Figure 6.3; here labeled on the plots with symbols for metamorphic zone color-coded by lithology. Abbreviations for zones are: Chl = Chlorite, Ank-Al = Ankerite–Albite, Ank-Ol = Ankerite–Oligoclase, Bio = Biotite, Amph = Amphibole, Diop = Diopside, Kyan = Kyanite.

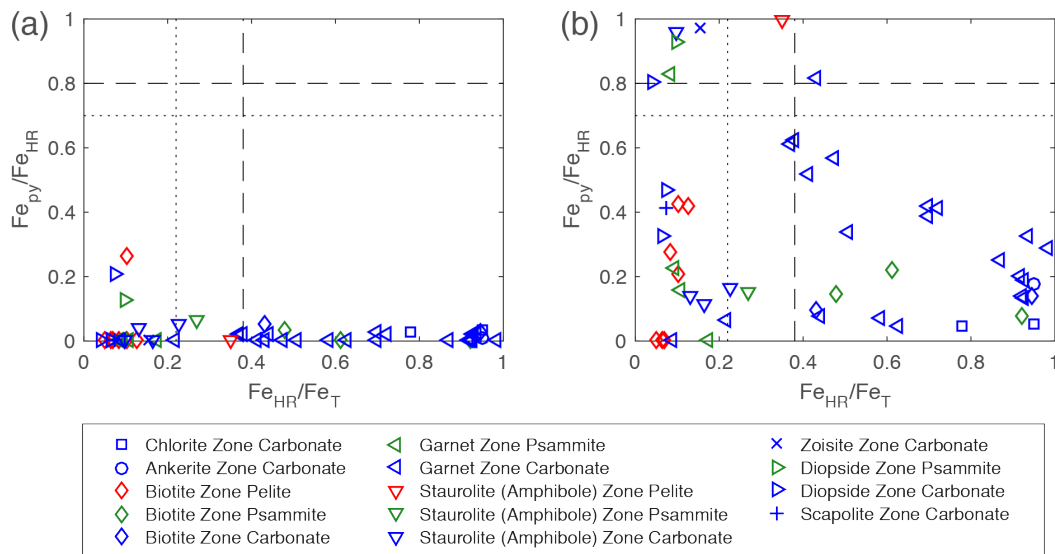


Figure 6.6: Waterville and Sangerville-Vassalboro Formation data plotted in iron speciation space. Legend is the same for both plots with different symbols representing the 8 different metamorphic zones color-coded by lithology. Staurolite (Amphibole) stands for the pelitic schist and carbonate facies respectively. (a) Pyrrhotite in the Fe_{carb} pool. (b) Pyrrhotite in the pyrite pool (Fe_{py}). Figures 6.7 and 6.8 show expanded plots for more detail.

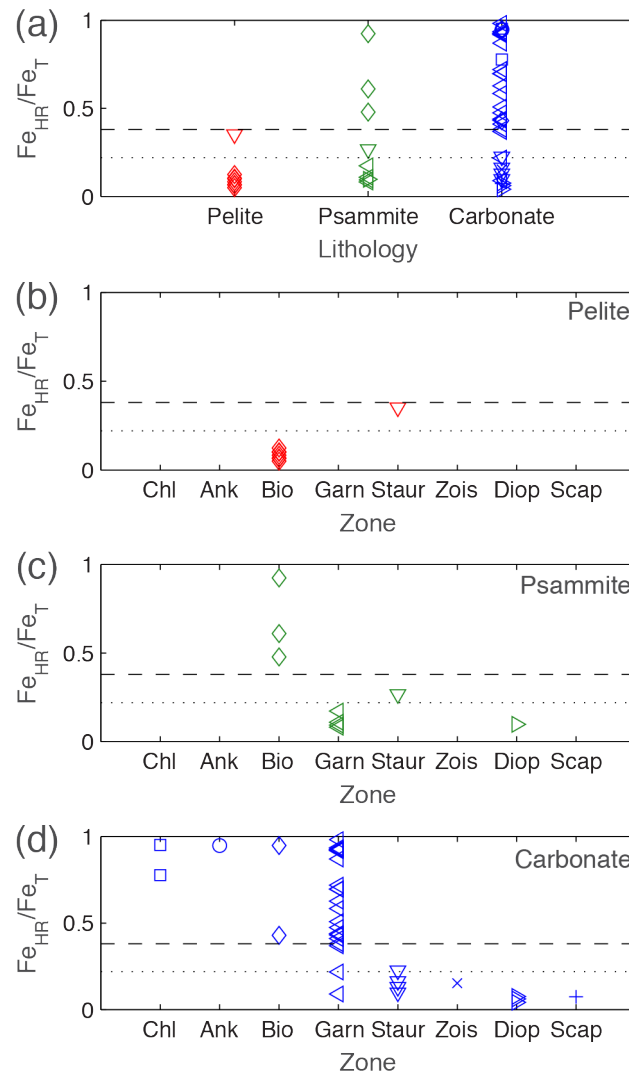


Figure 6.7: Highly reactive iron to total iron (Fe_{HR}/Fe_T) ratios in detail separated by lithology and zone for the Waterville and Sangerville-Vassalboro Formations. Same symbols as Figure 6.6; here labeled on the plots with symbols for metamorphic zone color-coded by lithology. Abbreviations for zones are: Chl = Chlorite, Ank = Ankerite, Bio = Biotite, Garn = Garnet, Staur = Staurolite (Amphibole), Zois = Zoisite, Diop = Diopside, Scap = Scapolite.

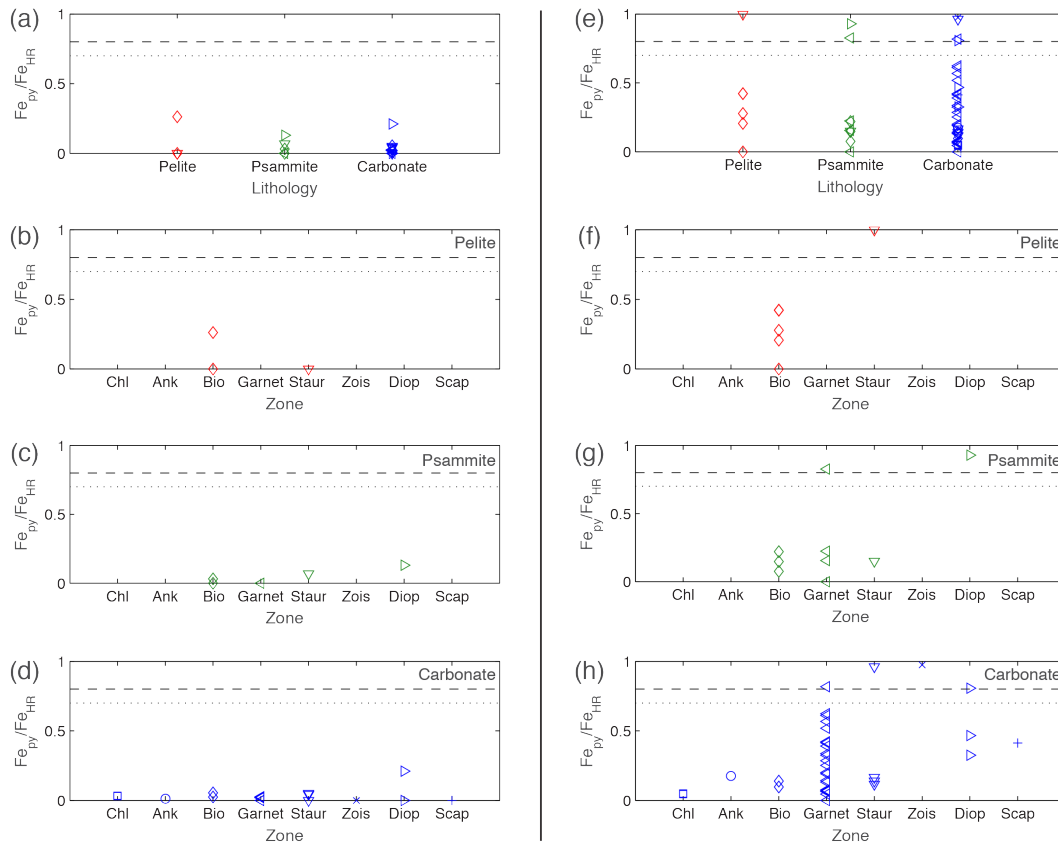


Figure 6.8: Pyrite to highly reactive iron (Fe_{py}/Fe_{HR}) ratios in detail separated by lithology and zone for the Waterville and Sangerville-Vassalboro Formations. (a-d) Pyrrhotite in the iron carbonate pool (Fe_{carb}). (e-h) Pyrrhotite in the pyrite pool (Fe_{py}). Same symbols as Figure 6.6; here labeled on the plots with symbols for metamorphic zone color-coded by lithology. Abbreviations for zones are: Chl = Chlorite, Ank = Ankerite, Bio = Biotite, Staur = Staurolite (Amphibole), Zois = Zoisite, Diop = Diopside, Scap = Scapolite.

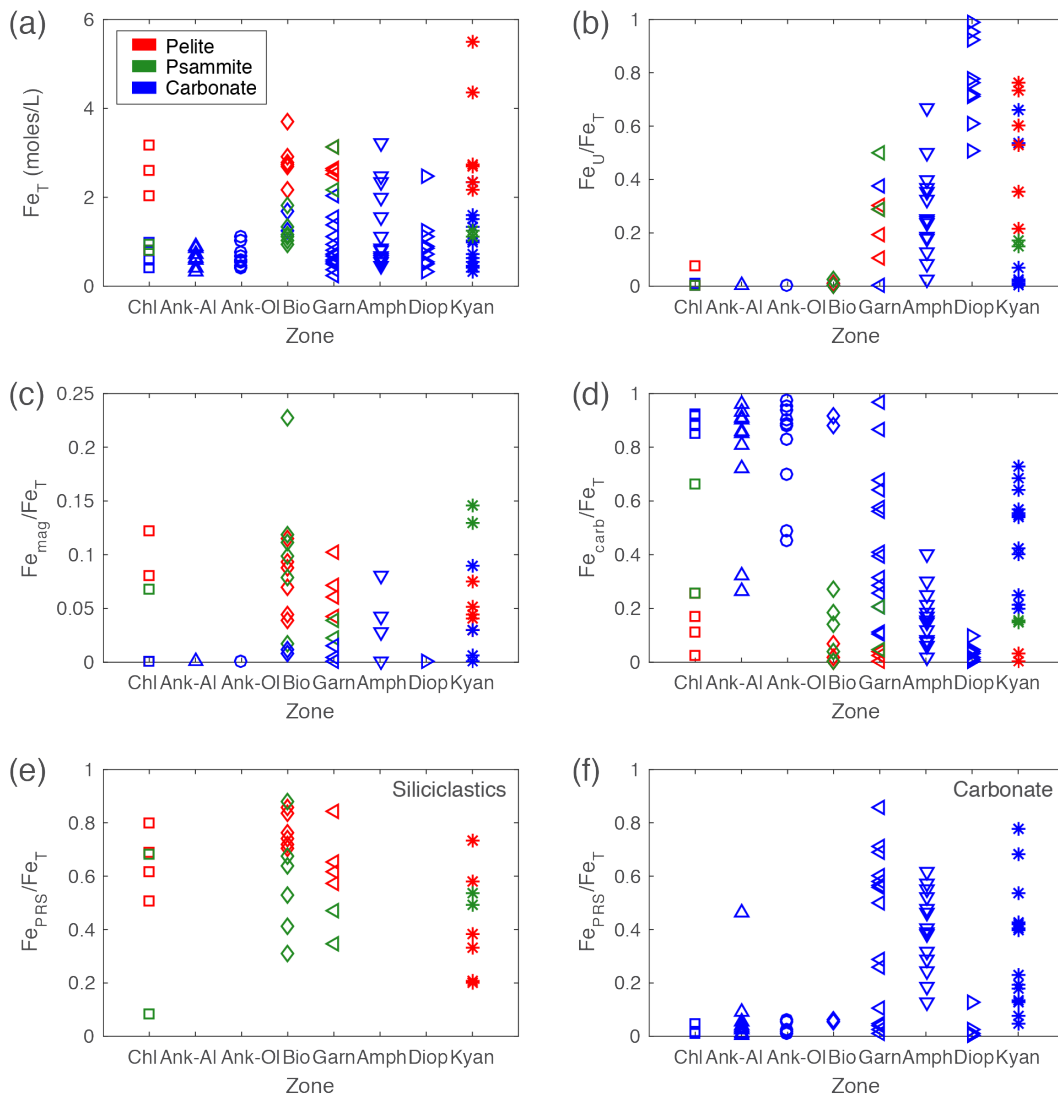


Figure 6.9: Different iron pools separated by metamorphic grade in samples from Waits River and Gile Mountain Formations. (a) Total iron (Fe_T). (b) Ratio of unreactive silicate iron to total iron (Fe_U/Fe_T). (c) Ratio of magnetite iron pool (entirely ilmenite here) to total iron (Fe_{mag}/Fe_T). Note this is at a different scale than (b-f). (d) Ratio of carbonate iron to total iron (Fe_{carb}/Fe_T). (e) Ratio of poorly reactive sheet silicates to total iron (Fe_{PRS}/Fe_T) for pelites and psammites. (f) Ratio of poorly reactive sheet silicates to total iron (Fe_{PRS}/Fe_T) for carbonate. Same symbols as Figure 6.3; lithology color codes in legend in (a) with symbols for metamorphic zone labeled on plots. Abbreviations for zones are: Chl = Chlorite, Ank-Al = Ankerite–Albite, Ank-Ol = Ankerite–Oligoclase, Bio = Biotite, Garn = Garnet, Amph = Amphibole, Diop = Diopside, Kyan = Kyanite. All data here is assuming pyrrhotite is in the pyrite pool (Fe_{py}).

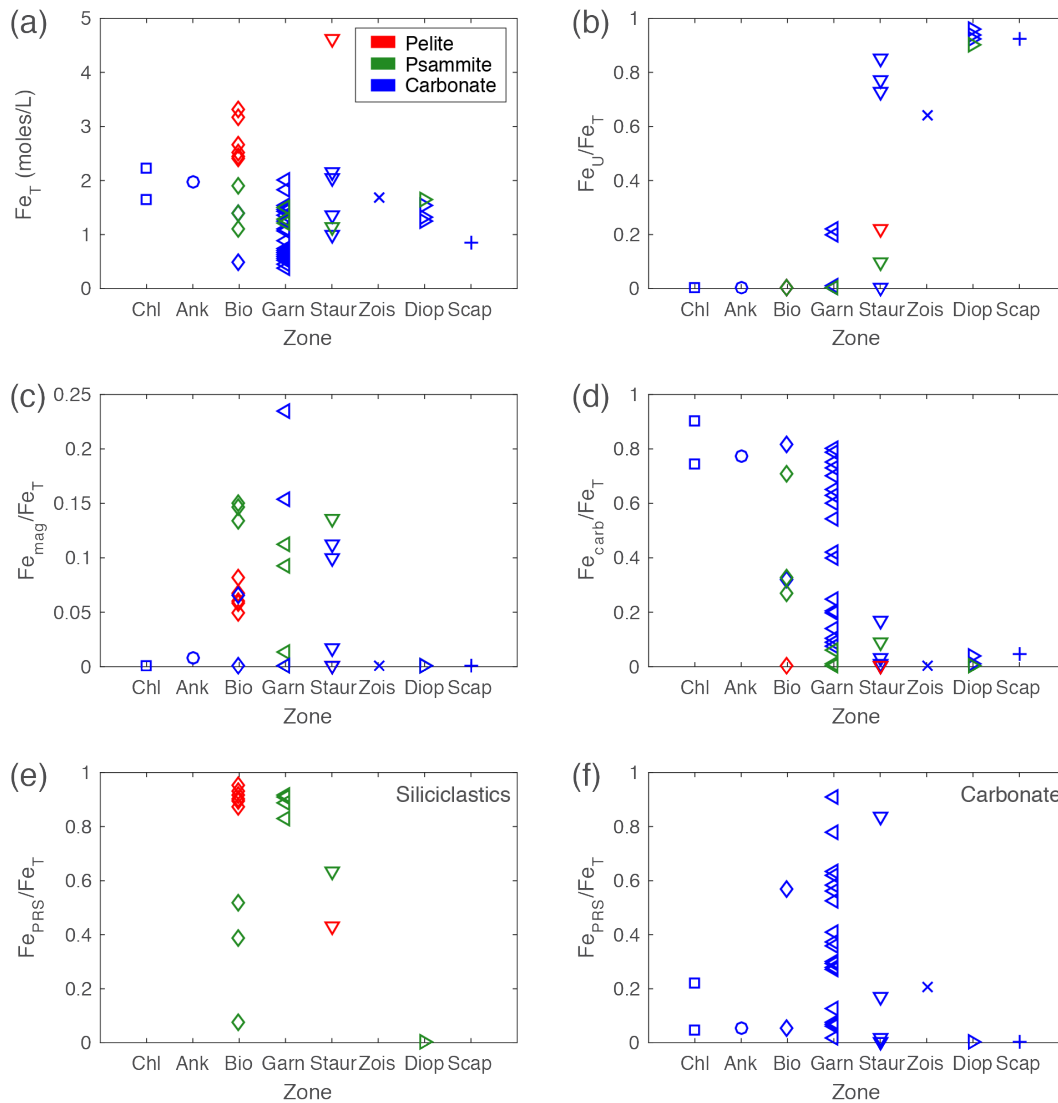


Figure 6.10: Different iron pools separated by metamorphic grade in samples from Waterville and Sangerville-Vassalboro Formations. (a) Total iron (Fe_T). (b) Ratio of unreactive silicate iron to total iron (Fe_U/Fe_T). (c) Ratio of magnetite iron pool (entirely ilmenite here) to total iron (Fe_{mag}/Fe_T). Note this is at a different scale than (b-f). (d) Ratio of carbonate iron to total iron (Fe_{carb}/Fe_T). (e) Ratio of poorly reactive sheet silicates to total iron (Fe_{PRS}/Fe_T) for pelites and psammites. (f) Ratio of poorly reactive sheet silicates to total iron (Fe_{PRS}/Fe_T) for carbonate. Same symbols as Figure 6.6; lithology color codes in legend in (a) with symbols for metamorphic zone labeled on plots. Abbreviations for zones are: Chl = Chlorite, Ank = Ankerite, Bio = Biotite, Garn = Garnet, Staur = Staurolite (Amphibole), Zois = Zoisite, Diop = Diopside, Scap = Scapolite. All data here is assuming pyrrhotite is in the pyrite pool (Fe_{py}).

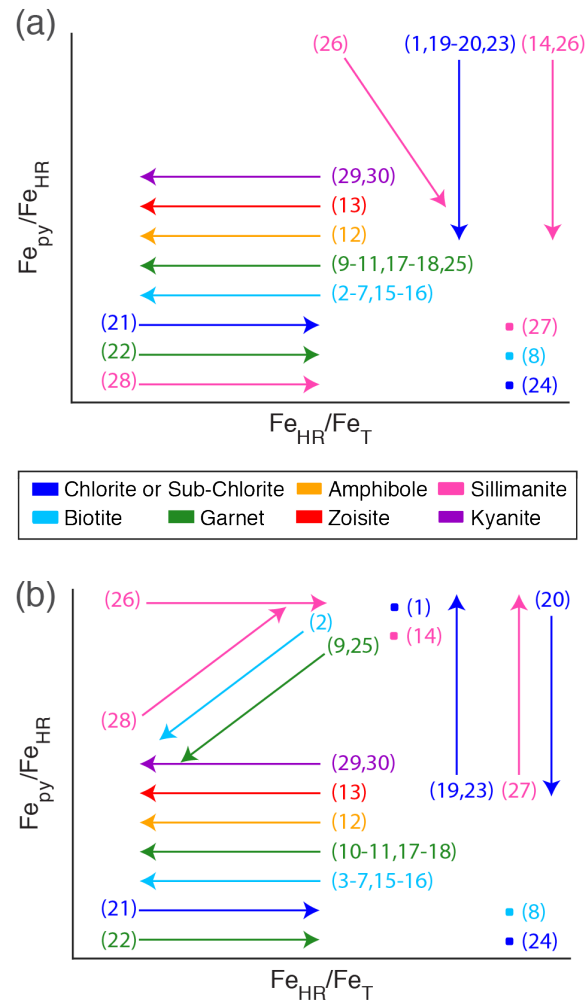


Figure 6.11: Example metamorphic reactions that transform iron between pools plotted in iron speciation place. Each vector shows the direction ratios will move as a given reaction progresses and are not quantitative. Vectors are color-coded by metamorphic zone when the reaction first occurs (cooler colors are lower metamorphic grade) with the same key for both plots. Numbers correspond to equations in Table 6.3 where more details on the reactions can be found. (a) Pyrrhotite in the Fe_{carb} pool. (b) Pyrrhotite in the pyrite pool (Fe_{py}).

6.10 Supplemental Figures

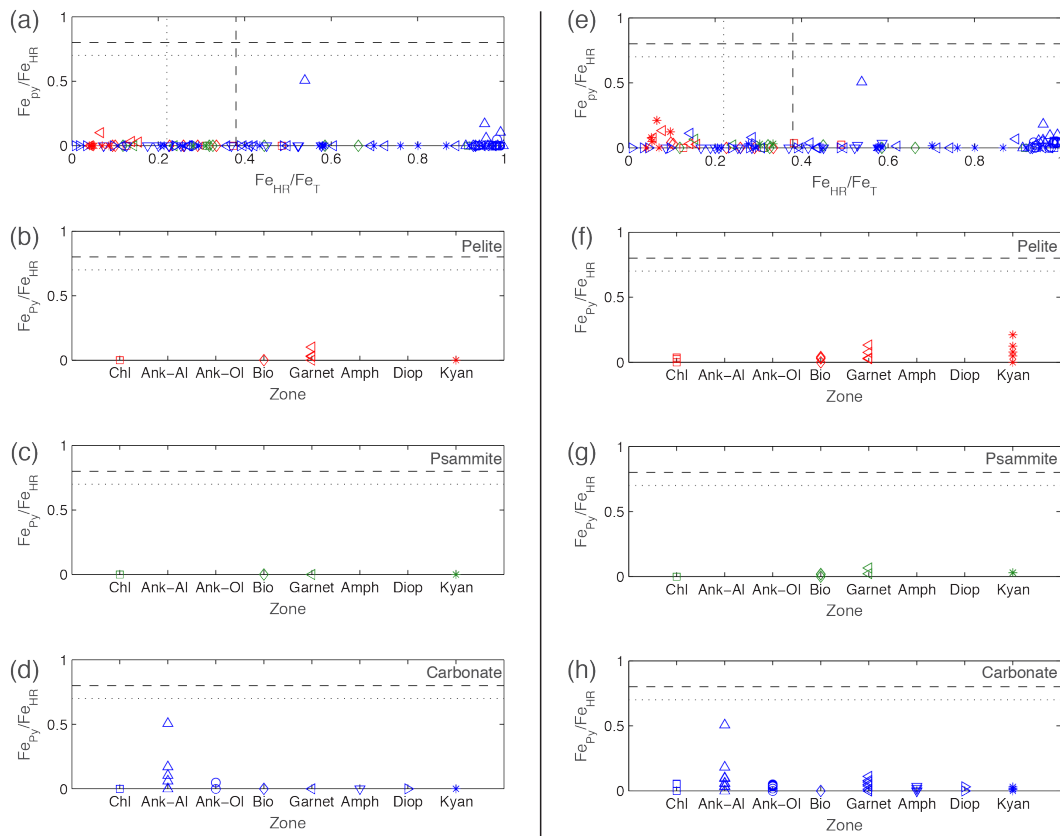


Figure S6.1: Waits River and Gile Mountain Formation data plotted in iron speciation space assuming pyrrhotite in the iron carbonate (Fe_{carb}) pool with details of Fe_{py}/Fe_{HR} ratios separated by lithology and zone. Same symbols as Figure 6.3; here labeled on the plots with different symbols representing the 8 different metamorphic zones color-coded by lithology. (a) Without trace minerals included. (b) With trace minerals included. Abbreviations for zones are: Chl = Chlorite, Ank-Al = Ankerite–Albite, Ank-Ol = Ankerite–Oligoclase, Bio = Biotite, Amph = Amphibole, Diop = Diopside, Kyan = Kyanite.

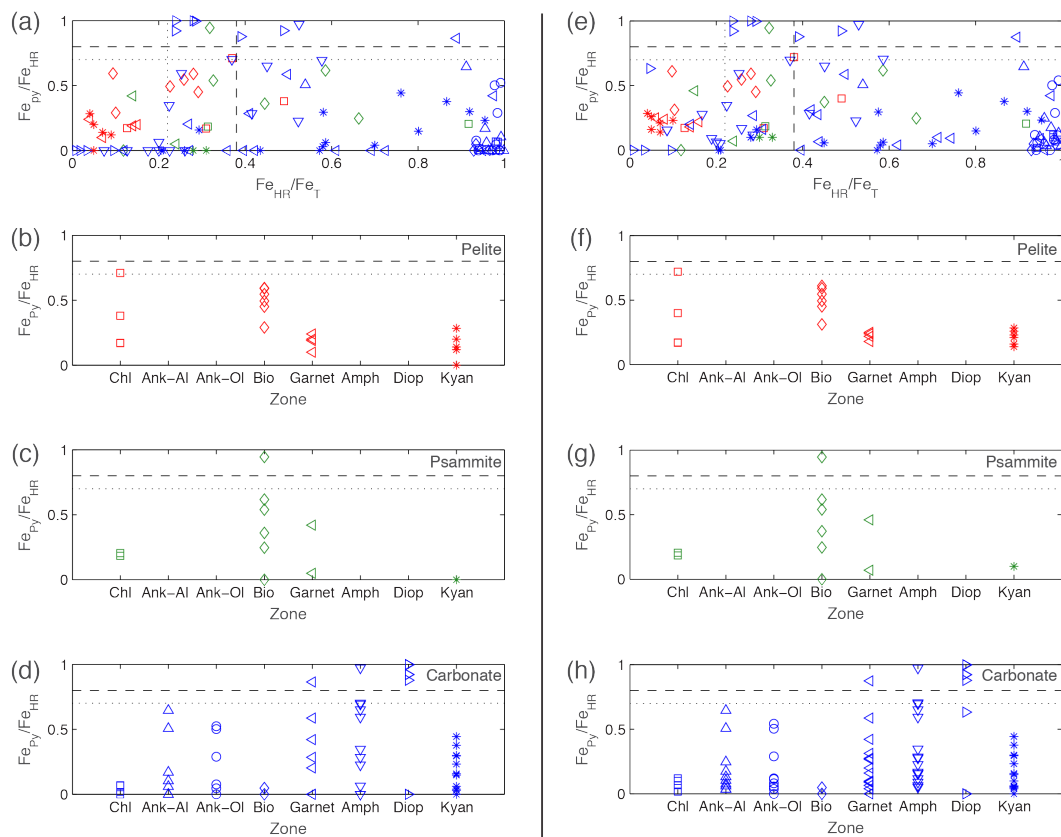


Figure S6.2: Waits River and Gile Mountain Formation data plotted in iron speciation space assuming pyrrhotite in the pyrite (Fe_{py}) pool with details of Fe_{py}/Fe_{HR} ratios separated by lithology and zone. Same symbols as Figure 6.3; here labeled on the plots with different symbols representing the 8 different metamorphic zones color-coded by lithology. (a) Without trace minerals included. (b) With trace minerals included. Abbreviations for zones are: Chl = Chlorite, Ank-Al = Ankerite-Albite, Ank-Ol = Ankerite-Oligoclase, Bio = Biotite, Amph = Amphibole, Diop = Diopside, Kyan = Kyanite.

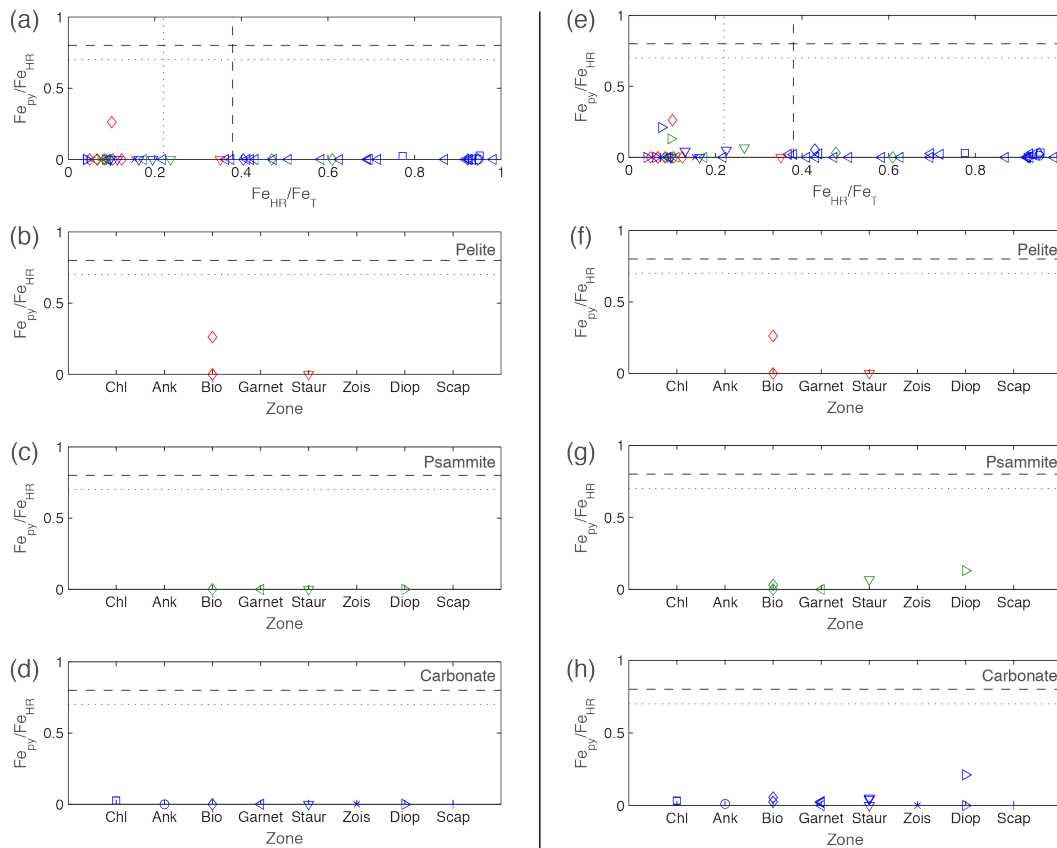


Figure S6.3: Waterville and Sangerville-Vassalboro Formation data plotted in iron speciation space assuming pyrrhotite in the iron carbonate (Fe_{carb}) pool with details of $\text{Fe}_{\text{py}}/\text{Fe}_{\text{HR}}$ ratios separated by lithology and zone. Same symbols as Figure 6.6; here labeled on the plots with different symbols representing the 8 different metamorphic zones color-coded by lithology. (a) Without trace minerals included. (b) With trace minerals included. Abbreviations for zones are: Chl = Chlorite, Ank = Ankerite, Bio = Biotite, Staur = Stauroilite (Amphibole), Zois = Zoisite, Diop = Diopside, Scap = Scapolite.

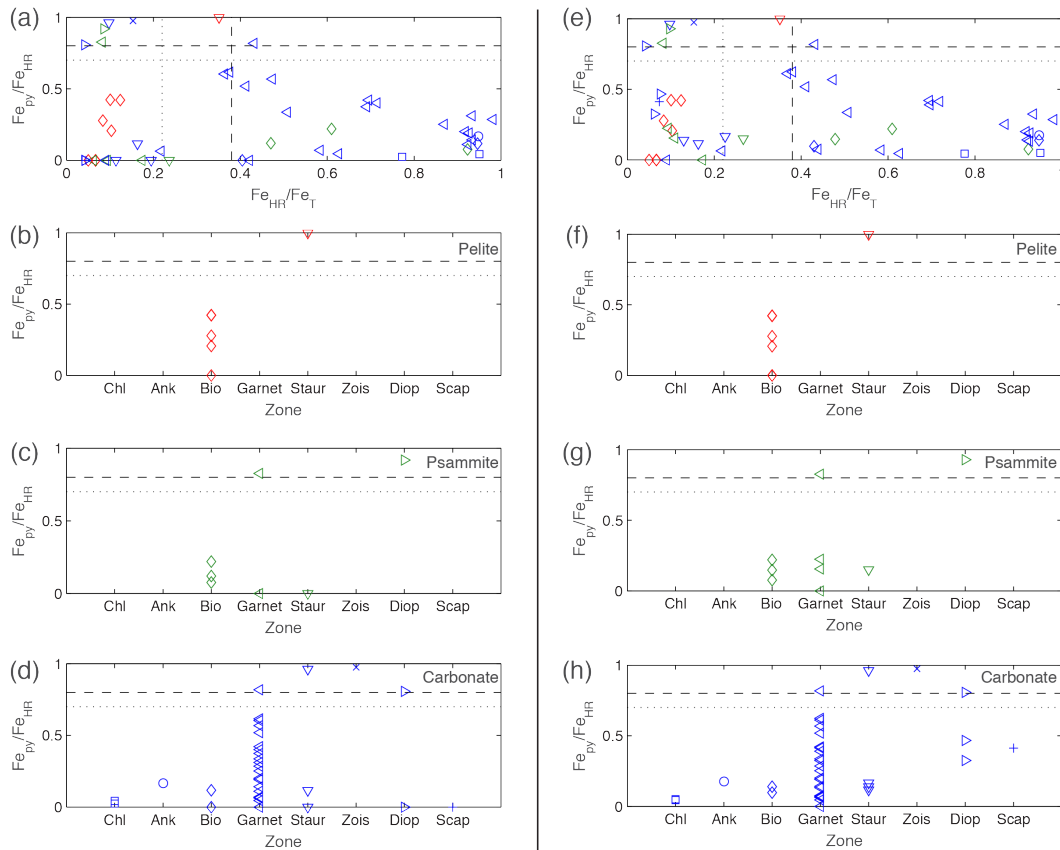


Figure S6.4: Waterville and Sangerville-Vassalboro Formation data plotted in iron speciation space assuming pyrrhotite in the pyrite (Fe_{py}) pool with details of $\text{Fe}_{\text{py}}/\text{Fe}_{\text{HR}}$ ratios separated by lithology and zone. Same symbols as Figure 6.6; here labeled on the plots with different symbols representing the 8 different metamorphic zones color-coded by lithology. (a) Without trace minerals included. (b) With trace minerals included. Abbreviations for zones are: Chl = Chlorite, Ank = Ankerite, Bio = Biotite, Staur = Staurolite (Amphibole), Zois = Zoisite, Diop = Diopside, Scap = Scapolite.

6.11 References

- Algoe, C., Stoops, G., Vandenberghe, R., and Van Ranst, E., 2012, Selective dissolution of Fe–Ti oxides—Extractable iron as a criterion for andic properties revisited: *Catena*, v. 92, p. 49-54.
- Anbar, A. D., 2008, Elements and evolution: *Science*, v. 322, no. 5907, p. 1481-1483.
- Anderson, T. F., and Raiswell, R., 2004, Sources and mechanisms for the enrichment of highly reactive iron in euxinic Black Sea sediments: *American Journal of Science*, v. 304, no. 3, p. 203-233.
- Arnold, G. L., Anbar, A., Barling, J., and Lyons, T., 2004, Molybdenum isotope evidence for widespread anoxia in mid-Proterozoic oceans: *Science*, v. 304, no. 5667, p. 87-90.
- Asael, D., Tissot, F. L., Reinhard, C. T., Rouxel, O., Dauphas, N., Lyons, T. W., Ponzevera, E., Liorzou, C., and Chéron, S., 2013, Coupled molybdenum, iron and uranium stable isotopes as oceanic paleoredox proxies during the Paleoproterozoic Shunga Event: *Chemical Geology*, v. 362, p. 193-210.
- Barnaby, R. J., and Rimstidt, J. D., 1989, Redox conditions of calcite cementation interpreted from Mn and Fe contents of authigenic calcites: *Geological Society of America Bulletin*, v. 101, no. 6, p. 795-804.
- Berner, R. A., 1970, Sedimentary pyrite formation: *American journal of science*, v. 268, no. 1, p. 1-23.
- , 1984, Sedimentary pyrite formation: an update: *Geochimica et Cosmochimica Acta*, v. 48, no. 4, p. 605-615.
- Bickle, M., Chapman, H., Ferry, J., Rumble, D., and Fallick, A., 1997, Fluid Flow and Diffusion in the Waterville Limestone, South—Central Maine: Constraints from Strontium, Oxygen and Carbon Isotope Profiles: *Journal of Petrology*, v. 38, no. 11, p. 1489-1512.
- Bucher, K., and Frey, M., 2002, *Petrogenesis of metamorphic rocks*, Berlin, Springer, Springer, Berlin, 341 p.:
- Burton, E. D., Bush, R. T., and Sullivan, L. A., 2006, Sedimentary iron geochemistry in acidic waterways associated with coastal lowland acid sulfate soils: *Geochimica et Cosmochimica Acta*, v. 70, no. 22, p. 5455-5468.
- Cabral, A., Creaser, R., Nägler, T., Lehmann, B., Voegelin, A., Belyatsky, B., Pašava, J., Gomes, A. S., Galbiatti, H., and Böttcher, M., 2013, Trace-element and

multi-isotope geochemistry of Late-Archean black shales in the Carajás iron-ore district, Brazil: *Chemical Geology*, v. 362, p. 91-104.

Canfield, D., 1998, A new model for Proterozoic ocean chemistry: *Nature*, v. 396, no. 6710, p. 450-453.

Canfield, D. E., and Berner, R. A., 1987, Dissolution and pyritization of magnetite in anoxic marine sediments: *Geochimica et Cosmochimica Acta*, v. 51, no. 3, p. 645-659.

Canfield, D. E., Raiswell, R., Westrich, J. T., Reaves, C. M., and Berner, R. A., 1986, The use of chromium reduction in the analysis of reduced inorganic sulfur in sediments and shales: *Chemical geology*, v. 54, no. 1, p. 149-155.

Clarkson, M., Poulton, S., Guilbaud, R., and Wood, R., 2014, Assessing the utility of Fe/Al and Fe-speciation to record water column redox conditions in carbonate-rich sediments: *Chemical Geology*, v. 382, p. 111-122.

Cloud, P. E., 1968, Atmospheric and Hydrospheric Evolution on the Primitive Earth: *Science*, v. 160, no. 3829, p. 729-736.

Connolly, J., and Cesare, B., 1993, C - O - H - S fluid composition and oxygen fugacity in graphitic metapelites: *Journal of metamorphic geology*, v. 11, no. 3, p. 379-388.

Cornwell, J. C., and Morse, J. W., 1987, The characterization of iron sulfide minerals in anoxic marine sediments: *Marine Chemistry*, v. 22, no. 2, p. 193-206.

Curtis, C., 1978, Possible links between sandstone diagenesis and depth-related geochemical reactions occurring in enclosing mudstones: *Journal of the Geological Society*, v. 135, no. 1, p. 107-117.

Dold, B., 2003, Speciation of the most soluble phases in a sequential extraction procedure adapted for geochemical studies of copper sulfide mine waste: *Journal of Geochemical Exploration*, v. 80, no. 1, p. 55-68.

Doll, C. G., Cady, W. M., Thompson Jr, J. B., and Billings, M. P., 1961, Centennial geologic map of Vermont: *Vermont Geol: Survey*, scale, v. 1, no. 250,000.

Ferry, J., 1976a, P, T, fCO₂ and fH₂O during metamorphism of calcareous sediments in the Waterville-Vassalboro area, south-central Maine: *Contributions to Mineralogy and Petrology*, v. 57, no. 2, p. 119-143.

Ferry, J. M., 1976b, Metamorphism of calcareous sediments in the Waterville-Vassalboro area, South-central Maine; mineral reactions and graphical analysis: *American Journal of Science*, v. 276, no. 7, p. 841-882.

Ferry, J. M., 1979, A map of chemical potential differences within an outcrop: *American Mineralogist*, v. 64, no. 9-10, p. 966-985.

Ferry, J. M., 1980, A comparative study of geothermometers and geobarometers in pelitic schists from south-central Maine: *American Mineralogist*, v. 65, p. 720-732.

Ferry, J. M., 1981, Petrology of graphitic sulfide-rich schists from south-central Maine: an example of desulfidation during prograde regional metamorphism: *American Mineralogist*, v. 66, p. 908-930.

-, 1983a, Mineral reactions and element migration during metamorphism of calcareous sediments from the Vassalboro Formation, south-central Maine: *American Mineralogist*, v. 68, no. 3-4, p. 334-354.

-, 1983b, Regional metamorphism of the Vassalboro Formation, south-central Maine, USA: a case study of the role of fluid in metamorphic petrogenesis: *Journal of the Geological Society*, v. 140, no. 4, p. 551-576.

-, 1984, A biotite isograd in south-central Maine, USA: mineral reactions, fluid transfer, and heat transfer: *Journal of Petrology*, v. 25, no. 4, p. 871-893.

-, 1988a, Contrasting mechanisms of fluid flow through adjacent stratigraphic units during regional metamorphism, south-central Maine, USA: *Contributions to Mineralogy and Petrology*, v. 98, no. 1, p. 1-12.

-, 1988b, Infiltration-driven metamorphism in northern New England, USA: *Journal of Petrology*, v. 29, no. 6, p. 1121-1159.

-, 1992, Regional metamorphism of the Waits River Formation, eastern Vermont: delineation of a new type of giant metamorphic hydrothermal system: *Journal of Petrology*, v. 33, no. 1, p. 45-94.

-, 1994, Overview of the petrologic record of fluid flow during regional metamorphism in northern New England: *American Journal of Science*, v. 294, no. 8, p. 905-988.

-, 2007, The role of volatile transport by diffusion and dispersion in driving biotite-forming reactions during regional metamorphism of the Gile Mountain Formation, Vermont: *American Mineralogist*, v. 92, no. 8-9, p. 1288-1302.

Fisher, G. W., and Karabinos, P., 1980, Stratigraphic sequence of the Gile Mountain and Waits River Formations near Royalton, Vermont: *Geological Society of America Bulletin*, v. 91, no. 5, p. 282-286.

French, B. M., 1973, Mineral assemblages in diagenetic and low-grade metamorphic iron-formation: *Economic Geology*, v. 68, no. 7, p. 1063-1074.

Gillett, S. L., 2003, Paleomagnetism of the Notch Peak contact metamorphic aureole, revisited: pyrrhotite from magnetite+ pyrite under submetamorphic conditions: *Journal of Geophysical Research: Solid Earth*, v. 108, no. B9.

Haase, C. S., 1982, Metamorphic petrology of the Negaunee Iron Formation, Marquette District, northern Michigan; mineralogy, metamorphic reactions, and phase equilibria: *Economic Geology*, v. 77, no. 1, p. 60-81.

Hall, A. J., 1986, Pyrite-pyrrhotite redox reactions in nature: *Mineralogical Magazine*, v. 50, p. 223-229.

Hatch, N. L., Jr., 1988, Some revisions to the stratigraphy and structure of the Connecticut Valley trough, eastern Vermont: *American Journal of Science*, v. 288, no. 10, p. 1041-1059.

Holland, H. D., 1984, *The chemical evolution of the atmosphere and oceans*, Princeton University Press.

Holland, T., and Powell, R., 1998, An internally consistent thermodynamic data set for phases of petrological interest: *Journal of Metamorphic Geology*, v. 16, no. 3, p. 309-343.

Hsieh, Y.-P., Chung, S.-W., Tsau, Y.-J., and Sue, C.-T., 2002, Analysis of sulfides in the presence of ferric minerals by diffusion methods: *Chemical Geology*, v. 182, no. 2, p. 195-201.

Hueber, F. M., Bothner, W. A., Hatch, N. L., Finney, S. C., and Aleinikoff, J. N., 1990, Devonian plants from southern Quebec and northern New Hampshire and the age of the Connecticut Valley trough: *American Journal of Science*, v. 290, no. 4, p. 360-395.

Johnson, J. E., Webb, S. M., Thomas, K., Ono, S., Kirschvink, J. L., and Fischer, W. W., 2013, Manganese-oxidizing photosynthesis before the rise of cyanobacteria: *Proceedings of the National Academy of Sciences*, v. 110, no. 28, p. 11238-11243.

Jones, J., 1972, An almandine garnet isograd in the Rogers Pass area, British Columbia: the nature of the reaction and an estimation of the physical conditions

during its formation: *Contributions to Mineralogy and Petrology*, v. 37, no. 4, p. 291-306.

Kendall, B., Creaser, R. A., Gordon, G. W., and Anbar, A. D., 2009, Re–Os and Mo isotope systematics of black shales from the Middle Proterozoic Velkerri and Wollongorang formations, McArthur Basin, northern Australia: *Geochimica et Cosmochimica Acta*, v. 73, no. 9, p. 2534-2558.

Klein, C., 1966, Mineralogy and petrology of the metamorphosed Wabush Iron Formation, southwestern Labrador: *Journal of Petrology*, v. 7, no. 2, p. 246-305.

Kopp, R. E., Kirschvink, J. L., Hilburn, I. A., and Nash, C. Z., 2005, The Paleoproterozoic snowball Earth: a climate disaster triggered by the evolution of oxygenic photosynthesis: *Proceedings of the National Academy of Sciences of the United States of America*, v. 102, no. 32, p. 11131-11136.

Léger, A., and Ferry, J., 1993, Fluid infiltration and regional metamorphism of the Waits River Formation, North - east Vermont, USA: *Journal of Metamorphic Geology*, v. 11, no. 1, p. 3-29.

Léger, A., and Ferry, J. M., 1991, Highly aluminous hornblende from low-pressure metacarbonates and a preliminary thermodynamic model for the Al content of calcific amphibole: *American Mineralogist*, v. 76, p. 1002-1017.

Leventhal, J., and Taylor, C., 1990, Comparison of methods to determine degree of pyritization: *Geochimica et Cosmochimica Acta*, v. 54, no. 9, p. 2621-2625.

Li, C., Planavsky, N. J., Love, G. D., Reinhard, C. T., Hardisty, D., Feng, L., Bates, S. M., Huang, J., Zhang, Q., and Chu, X., 2015, Marine redox conditions in the middle Proterozoic ocean and isotopic constraints on authigenic carbonate formation: Insights from the Chuanlinggou Formation, Yanshan Basin, North China: *Geochimica et Cosmochimica Acta*, v. 150, p. 90-105.

Li, Y., and Schoonmaker, J., 2003, Chemical Composition and Mineralogy of Marine Sediments, *in* Mackenzie, F. T., ed., *Sediments, Diagenesis, and Sedimentary Rocks: Treatise on Geochemistry, Volume 7*, p. 1-35.

Lodders, K., and Fegley, B., 1997, An oxygen isotope model for the composition of Mars: *Icarus*, v. 126, no. 2, p. 373-394.

Lyons, J. B., 1955, Geology of the Hanover quadrangle, New Hampshire-Vermont: *Geological Society of America Bulletin*, v. 66, no. 1, p. 105-146.

März, C., Poulton, S., Beckmann, B., Küster, K., Wagner, T., and Kasten, S., 2008, Redox sensitivity of P cycling during marine black shale formation:

dynamics of sulfidic and anoxic, non-sulfidic bottom waters: *Geochimica et Cosmochimica Acta*, v. 72, no. 15, p. 3703-3717.

Moench, R. H., Boone, G., Bothner, W., Boudette, E., Hatch Jr, N., Hussey III, A., and Marvinney, R., 1995, *Geologic Map of the Sherbrooke-Lewiston Area, Maine, New Hampshire, and Vermont, United States, and Quebec, Canada*: US Geological Survey.

Nesbitt, B., and Kelly, W., 1980, Metamorphic zonation of sulfides, oxides, and graphite in and around the orebodies at Ducktown, Tennessee: *Economic Geology*, v. 75, no. 7, p. 1010-1021.

Osberg, P., 1988, Geologic relations within the shale-wacke sequence in south-central Maine: *Studies in Maine geology*, v. 1, p. 51-73.

Osberg, P. H., 1968, *Stratigraphy, structural geology, and metamorphism of the Waterville-Vassalboro area, Maine*, Maine Geological Survey.

Osberg, P. H., Tull, J. F., Robinson, P., Hon, R., and Butler, J. R., 1989, The Acadian orogen: The Appalachian–Ouachita orogen in the United States, *The geology of North America*: Geological Society of America, Boulder, v. 2, p. 179-232.

Pankiwskyj, K. A., Ludman, A., Griffin, J. R., and Berry, W., 1976, Stratigraphic relationships on the southeast limb of the Merrimack synclinorium in central and west-central Maine: *Geological Society of America Memoirs*, v. 146, p. 263-280.

Partin, C., Bekker, A., Planavsky, N., and Lyons, T., 2015, Euxinic conditions recorded in the ca. 1.93 Ga Bravo Lake Formation, Nunavut (Canada): Implications for oceanic redox evolution: *Chemical Geology*, v. 417, p. 148-162.

Penniston-Dorland, S. C., and Ferry, J. M., 2006, Development of spatial variations in reaction progress during regional metamorphism of micaceous carbonate rocks, northern New England: *American Journal of Science*, v. 306, no. 7, p. 475-524.

-, 2008, Element mobility and scale of mass transport in the formation of quartz veins during regional metamorphism of the Waits River Formation, east-central Vermont: *American Mineralogist*, v. 93, no. 1, p. 7-21.

Poulton, S., and Raiswell, R., 2002, The low-temperature geochemical cycle of iron: from continental fluxes to marine sediment deposition: *American Journal of Science*, v. 302, no. 9, p. 774-805.

- Poulton, S. W., and Canfield, D. E., 2005, Development of a sequential extraction procedure for iron: implications for iron partitioning in continentally derived particulates: *Chemical Geology*, v. 214, no. 3, p. 209-221.
- , 2011, Ferruginous conditions: a dominant feature of the ocean through Earth's history: *Elements*, v. 7, no. 2, p. 107-112.
- Praharaj, T., and Fortin, D., 2004, Determination of acid volatile sulfides and chromium reducible sulfides in Cu-Zn and Au mine tailings: Water, air, and soil pollution, v. 155, no. 1-4, p. 35-50.
- Raiswell, R., and Berner, R. A., 1985, Pyrite formation in euxinic and semi-euxinic sediments: *American Journal of Science*, v. 285, no. 8, p. 710-724.
- Raiswell, R., Buckley, F., Berner, R. A., and Anderson, T., 1988, Degree of pyritization of iron as a paleoenvironmental indicator of bottom-water oxygenation: *Journal of Sedimentary Research*, v. 58, no. 5.
- Raiswell, R., Canfield, D., and Berner, R., 1994, A comparison of iron extraction methods for the determination of degree of pyritisation and the recognition of iron-limited pyrite formation: *Chemical Geology*, v. 111, no. 1, p. 101-110.
- Raiswell, R., and Canfield, D. E., 1998, Sources of iron for pyrite formation in marine sediments: *American Journal of Science*, v. 298, no. 3, p. 219-245.
- , 2012, The iron biogeochemical cycle past and present: *Geochemical Perspectives*, v. 1, no. 1, p. 1-2.
- Raiswell, R., Newton, R., and Wignall, P., 2001, An indicator of water-column anoxia: resolution of biofacies variations in the Kimmeridge Clay (Upper Jurassic, UK): *Journal of Sedimentary Research*, v. 71, no. 2, p. 286-294.
- Raiswell, R., Reinhard, C. T., Derkowski, A., Owens, J., Bottrell, S. H., Anbar, A. D., and Lyons, T. W., 2011, Formation of syngenetic and early diagenetic iron minerals in the late Archean Mt. McRae Shale, Hamersley Basin, Australia: New insights on the patterns, controls and paleoenvironmental implications of authigenic mineral formation: *Geochimica et Cosmochimica Acta*, v. 75, no. 4, p. 1072-1087.
- Reinhard, C. T., Lyons, T. W., Rouxel, O., Asael, D., Dauphas, N., and Kump, L. R., 2013, 7.10.4 Iron Speciation and Isotope Perspectives on Palaeoproterozoic Water Column Chemistry, *in* Melezhik, V., Prave, A.R., Hanski, E.J., Fallick, A.E., Lepland, A., Kump, L.R., Strauss, H., ed., *Reading the Archive of Earth's Oxygenation*, Volume 3: Berlin Heidelberg, Springer, p. 1483-1492.

- Reinhard, C. T., Raiswell, R., Scott, C., Anbar, A. D., and Lyons, T. W., 2009, A late Archean sulfidic sea stimulated by early oxidative weathering of the continents: *Science*, v. 326, no. 5953, p. 713-716.
- Reuschel, M., Melezhik, V., and Strauss, H., 2012, Sulfur isotopic trends and iron speciation from the c. 2.0 Ga Pilgūjärvi Sedimentary Formation, NW Russia: *Precambrian Research*, v. 196, p. 193-203.
- Robie, R. A., Bethke, P. M., and Beardsley, K. M., 1967, Selected X-ray crystallographic data, molar volumes, and densities of minerals and related substances: US Government Printing Office.
- Roscoe, S., 1969, Huronian rocks and uraniferous conglomerates in the Canadian Shield: Geological Survey of Canada.
- Schumann, R., Stewart, W., Miller, S., Kawashima, N., Li, J., and Smart, R., 2012, Acid-base accounting assessment of mine wastes using the chromium reducible sulfur method: *Science of the Total Environment*, v. 424, p. 289-296.
- Shen, Y., Canfield, D. E., and Knoll, A. H., 2002, Middle Proterozoic ocean chemistry: evidence from the McArthur Basin, northern Australia: *American Journal of Science*, v. 302, no. 2, p. 81-109.
- Sleep, N. H., and Bird, D. K., 2008, Evolutionary ecology during the rise of dioxygen in the Earth's atmosphere: *Philosophical Transactions of the Royal Society of London B: Biological Sciences*, v. 363, no. 1504, p. 2651-2664.
- Spear, F. S., and Harrison, T. M., 1989, Geochronologic studies in central New England I: Evidence for pre-Acadian metamorphism in eastern Vermont: *Geology*, v. 17, no. 2, p. 181-184.
- Sperling, E. A., Wolock, C. J., Morgan, A. S., Gill, B. C., Kunzmann, M., Halverson, G. P., Macdonald, F. A., Knoll, A. H., and Johnston, D. T., 2015, Statistical analysis of iron geochemical data suggests limited late Proterozoic oxygenation: *Nature*, v. 523, no. 7561, p. 451-454.
- Thompson, J., and Norton, S. A., 1968, Paleozoic regional metamorphism in New England and adjacent areas, *in* E-an Zen, W. S. W., J.B. Hadley,, and and J.B. Thompson, J., eds., *Studies of Appalachian Geology: Northern and Maritime*: New York, Wiley, p. 319-327.
- Thompson, J. B., Jr., Robinson, P., Clifford, T. N., and Trask Jr, N. J., 1968, Nappes and gneiss domes in west-central New England, *in* E-an Zen, W. S. W., and J.B. Hadley, a. J. B. T., Jr., eds., *Studies of Appalachian Geology: Northern and Maritime*: New York, Wiley, p. 203-218.

- Tomkins, A. G., 2010, Windows of metamorphic sulfur liberation in the crust: implications for gold deposit genesis: *Geochimica et Cosmochimica Acta*, v. 74, no. 11, p. 3246-3259.
- Tracy, R. J., and Robinson, P., 1988, Silicate-sulfide-oxide-fluid reactions in granulite-grade pelitic rocks, central Massachusetts: *American Journal of Science*, v. 288, p. 45-74.
- Tucker, R., Osberg, P., and Berry, H., 2001, The geology of a part of Acadia and the nature of the Acadian orogeny across central and eastern Maine: *American Journal of Science*, v. 301, no. 3, p. 205-260.
- Walker, R., and James, N., 1992, Facies models: Response to sea level change, St. John's, Newfoundland, Geological Association of Canada, John's, Newfoundland, Geological Association of Canada.
- Warren, J., 2000, Dolomite: occurrence, evolution and economically important associations: *Earth-Science Reviews*, v. 52, no. 1, p. 1-81.
- Watkins, R., 1996, Skeletal composition of Silurian benthic marine faunas: *Palaios*, p. 550-558.
- Whitney, D. L., and Evans, B. W., 2010, Abbreviations for names of rock-forming minerals: *American mineralogist*, v. 95, no. 1, p. 185.
- Wilkin, R., and Barnes, H., 1997, Formation processes of framboidal pyrite: *Geochimica et Cosmochimica Acta*, v. 61, no. 2, p. 323-339.
- Wilkin, R., Barnes, H., and Brantley, S., 1996, The size distribution of framboidal pyrite in modern sediments: an indicator of redox conditions: *Geochimica et Cosmochimica Acta*, v. 60, no. 20, p. 3897-3912.
- Williams, R. P. J., and Frausto Da Silva, J. J. R., 2003, Evolution was chemically constrained: *Journal of Theoretical Biology*, v. 220, no. 3, p. 323-343.
- Williamson, A., Conlan, B., Hillier, W., and Wydrzynski, T., 2011, The evolution of Photosystem II: insights into the past and future: *Photosynthesis research*, v. 107, no. 1, p. 71-86.
- Wing, B. A., Ferry, J. M., and Harrison, T. M., 2003, Prograde destruction and formation of monazite and allanite during contact and regional metamorphism of pelites: petrology and geochronology: *Contributions to Mineralogy and Petrology*, v. 145, no. 2, p. 228-250.
- Woodland, B. G., 1977, Structural analysis of the Silurian-Devonian rocks of the Royalton area, Vermont: *Geological Society of America Bulletin*, v. 88, no. 8, p. 1111-1123.

Zerkle, A. L., House, C. H., and Brantley, S. L., 2005, Biogeochemical signatures through time as inferred from whole microbial genomes: *American Journal of Science*, v. 305, no. 6-8, p. 467-502.

Zhou, T., Phillips, G. N., Dong, G., and Myers, R. E., 1995, Pyrrhotite in the Witwatersrand gold fields, South Africa: *Economic Geology*, v. 90, no. 8, p. 2361-2369.